ELSEVIER

Journal of Nuclear Materials 297 (2001) 176–205

journal of nuclear materials

www.elsevier.com/locate/jnucmat

Post-irradiation examination of high burnup Mg doped UO_2 in comparison with undoped UO_2, Mg–Nb doped UO_2 and Ti doped UO_2

Takeo Fujino [a,*], Tetsuo Shiratori [b], Nobuaki Sato [a], Kousaku Fukuda [b], Kohta Yamada [a], Hiroyuki Serizawa [b]

[a] *Institute for Advanced Materials Processing, Tohoku University, 2-1-1 Katahira, Aoba-ku, Sendai 980-8577, Japan*
[b] *Japan Atomic Energy Research Institute, Tokai-mura, Naka-gun, Ibaraki 319-1195, Japan*

Received 25 September 2000; accepted 2 May 2001

Abstract

The pellets of UO_2, magnesium doped UO_2 (Mg–UO_2), magnesium and niobium doped UO_2 (Mg–Nb–UO_2) and titanium doped UO_2 (Ti–UO_2) were irradiated to burnups ranging from 19 to 94 GWd/tU at temperatures 550–930°C. The solubility of magnesium in UO_2 was low around 2 mol%. The addition of magnesium and titanium caused to form large grain sized pellet on sintering. The swelling of pellets during irradiation was unchanged by magnesium addition below 60 GWd/tU in agreement with the literature rate for UO_2. The thermal conductivity of unirradiated Mg–UO_2 was higher than that of undoped UO_2, which seemed to also hold for irradiated specimens. Pellet fracturing occurred by irradiation mainly by thermal stress. The undoped and metal doped UO_2 pellets in the 84–94 GWd/tU range at the irradiation temperatures of 560–640°C showed large bubbles and sub-divided grains of sub-micron size and the rim structure formation all over the surface. The xenon release from the pellets during irradiation increased with increasing burnup. In the fuels of close burnups, the xenon release increased rapidly with increasing temperature above about 600°C. At high burnups, the effect of metal addition seemed to recede unclear perhaps due to the formation of heavily damaged fuel matrix.

PACS: 28.41.Bm

1. Introduction

The effect of the addition of metal oxides to UO_2 has been studied since 1960s with the aim to improve the irradiation behavior of UO_2 fuel in LWR. Lanthanide (or actinide) elements, alkaline-earth metals and some transition metals form solid solutions with UO_2 on heating under appropriately low oxygen partial pressures. The formed solid solutions are usually of substitutional type which are expressed as $A_yU_{1-y}O_{2+x}$, and they show higher oxygen potentials ($\Delta\overline{G}_{O_2}$) than undoped UO_{2+x} at the same O/M (M = A + U) atom ratio. This difference has been considered to be caused mainly by the increase of the configurational entropy [1,2].

The same low oxygen potential as UO_{2+x} can, however, be attained also by solid solutions at lower O/M ratios. The solid solutions can take such low O/M ratios because their stability range extends to O/M ratios lower than 2.0, in contrast to UO_{2+x} of which the lower limit of oxygen nonstoichiometry is 2.0 ($x = 0$) below 1400°C [3]. Actually, very low $\Delta\overline{G}_{O_2}$ has been measured for $Pu_yU_{1-y}O_{2+x}$ (MOX) around O/M = 1.96 at 1200°C [4]. Another notable feature of the solid solutions is the gentler slope of the curve of $\Delta\overline{G}_{O_2}$ against O/M ratio in low $\Delta\overline{G}_{O_2}$ region [5], which suggests a slower $\Delta\overline{G}_{O_2}$ increase when the O/M ratio increases by high burnups.

* Corresponding author. Tel.: +81-22 217 5163; fax: +81-22 217 5164.
E-mail address: fujino@iamp.tohoku.ac.jp (T. Fujino).

0022-3115/01/$ - see front matter
PII: S0022-3115(01)00609-2

On the other hand, the addition of metal oxides is known to give large grain sized pellets on fabrication. With such pellets, the release rate of fission gases during irradiation should be reduced because of longer path for the fission gases to attain grain boundaries [6]. This effect has been studied for a large number of metal oxides, viz. TiO_2 [7–11], Nb_2O_5 [9,12–14], V_2O_5 [9,15], Cr_2O_3 [16,17], La_2O_3 [12], MgO [7,17], CaO–TiO_2 [18,19]. The grain size was observed to increase markedly by the addition of TiO_2, Nb_2O_5 and V_2O_5. At higher metal concentrations, a pronounced sweeping of the fine pores smaller than 2 μm has been observed [19]. However for Cr_2O_3, no significant decrease in the gas release rate was found for the fuel up to the maximum burnup of 0.45% FIMA at 1500°C, although the addition of 0.9 mol% chromium yielded the pellets with the grain size about seven times greater than the undoped UO_2 [16]. This result is thought to be due to enhanced rare-gas diffusion coefficient and reduced grain boundary energy in the chromium doped fuel. The diffusion coefficient of ^{133}Xe for UO_2 doped with Cr_2O_3 (0.12 mol%) was measured to be about three times as high as that of the undoped UO_2 fuel [17]. The large grain size does not always give a low release rate.

In the case of MgO addition, substantial reduction of the fission gas release rate has been observed [20]. The reduction factor was 2.5 for the 5 mol% MgO doped UO_2 fuel (grain size: 35 μm) at a burnup of 28.5 GWd/tU [21]. The diffusion coefficient of ^{133}Xe for 3.4 mol% MgO doped UO_2 pellet did not differ significantly from that of the undoped UO_2 [17]. The small neutron absorption cross-sections of natural isotopes of magnesium, i.e. ^{24}Mg, ^{25}Mg and ^{26}Mg certify a good neutron economy in reactor.

The solubility of magensium in UO_2 is as high as 33.3 mol% at 1200°C if the oxygen partial pressure is 10^{-1}–1 Pa [22,23]. However, it decreases with decreasing oxygen partial pressure [24]. The reported solubility values are not in good agreement [21,25]. But according to our data [26], the solubility again increased to about 10 mol% Mg below 10^{-6} Pa. For magnesium solid solution, the O/M ratio which yields the steepest $\Delta\overline{G}_{O_2}$ change is markedly lowered from 2.0 [26–28]. This is the different behavior from the most other solid solutions, and the contribution of the shift to better fuel performance may be expected. The effect of large grain size to keep the fission gases would also be related to the oxygen potential. Then, following the preceding papers on the irradiation experiment of magnesium solid solutions [29,30], we report here the detailed results of the post-irradiation examinations carried out for magnesium doped UO_2 fuel together with those for undoped UO_2, Mg–Nb–UO_2 and Ti–UO_2 including the fission gas release data. The metal doped pellets were irradiated up to a high burnup of 94 GWd/tU at various temperatures ranging from 550°C to 930°C.

2. Experimental

2.1. Materials used

The oxides of uranium with 5.973, 10.000 and 19.750 ^{235}U enrichment were imported from USA in a chemical form of U_3O_8. They were reduced to UO_2 by heating in a stream of 4%H_2–He at 700°C. Heavy MgO of guaranteed reagent grade (CaO < 0.05%, heavy metals < 0.005%) and Nb_2O_5 of 99.9% purity were purchased from Wako Pure Chemicals Industries. Finely divided titanium metal (−100 mesh) of 99.99% purity was obtained from Soekawa Chemical. The 4%H_2–He mixed gas of 99.999% purity was obtained from Nippon Sanso and used as-received.

2.2. Preparation of metal doped uranium dioxides

Magnesium uranates, $MgUO_4$ and MgU_3O_{10}, were prepared by heating the respective mixtures of calculated amounts of MgO and UO_2 in air at 850°C. For preparing the metal doped UO_2, first the calculated amounts of MgO, $MgUO_4$, MgU_3O_{10}, Nb_2O_5 or titanium metal powder were intimately mixed with UO_2 in an agate mortar. Four types of samples were prepared for irradiation. They were: undoped UO_2, magnesium doped UO_2 (magnesium concentrations: 2.5, 5, 10 and 15 mol%), 5 mol% magnesium and 5 mol% niobium doped UO_2 (5%Mg–5%Nb–UO_2) and 3.5 mol% titanium doped UO_2 (3.5%Ti–UO_2). To change burnup, the samples with uranium enrichments of 6%, 10% and 20% were prepared. The mixture powder was pressed into pellets of 3 mm diameter and about 1 mm thickness. The pellets in Mo crucibles were heated in a tungsten-mesh resistance furnace in a stream of 4%H_2–He mixed gas. The heating condition was varied with samples. For undoped UO_2 and magnesium doped UO_2, the mixture pellets were heated at 1710°C for 5 h. For 5%Mg–5%Nb–UO_2, they were heated at 1500°C for 0.5 h. The 3.5%Ti–UO_2 pellets were heated at 1550°C for either 10 or 20 h. The sintered pellets shrank to about 2.5 mm∅.

2.3. X-ray diffraction analysis

X-ray powder diffractometry for unirradiated samples was carried out with a Rigaku Rotaflex RU-200B diffractometer using CuKα radiation (40 kV, 120 mA) monochromatized with curved pyrolytic graphite. The slit system used was 1°–0.5 mm–1°–0.6 mm. The measurement was made in the 2θ range from 10° to 120° with a scanning rate of 1°(2θ)/min.

2.4. Density measurement

The density of unirradiated and irradiated pellets was measured by the fluid gravimetry method using diiodomethane ($d^{20} = 3.3212$ g/cm^3). The sample with the weights ranging from ~0.05 g (one pellet) to 0.2 g (four pellets) was precisely weighed in a basket made of thin stainless steel mesh (0.3 g) first in air and then immersing in diiodomethane at 20°C.

2.5. Grain size measurement

The grain size of the unirradiated solid solutions was measured metallographically using an optical microscope. First, from the sample pellet fixed in resin, a section for inspection was polished out. Then, its surface was etched in a solution of H_2O_2 and H_2SO_4 (volume ratio 8:1) for 15–30 s at room tempeature. From the photographs of ×200 magnification, the grain size was calculated using the linear intercept method with $l\pi/(2n)$, where l is the length of measurement and n is the number of particles in length l.

2.6. SEM and EPMA analyses

SEM and EPMA analyses were carried out with a JEOL JSM-5400 scanning electron microscope and a Shimadzu EPM-810 electron probe microanalyzer, respectively. The sample pellet fixed in resin was cut and polished to have the surface. Thin gold film was formed on the surface by vacuum evaporation for electrical conductivity. SEM observation was performed for this sample up to a magnification of ×7000. By EPMA, qualitative analysis of uranium, magnesium, niobium and titanium was made. Also, the existing state of metals and their structure were observed.

2.7. Thermal diffusivity measurement

The thermal diffusivity of the unirradiated and irradiated pellets was measured by the laser-flash method with an ULVAC, TC-7000 apparatus in vacuum. The temperature was measured by In–Sb infrared detector. Measurements were made every 200°C interval between 200°C and 1400°C. Since no significant difference was found to exist between the unpolished and polished samples, most measurements were performed on the unpolished surface. The obtained data were analyzed by the logarithm method.

3. Observation of sintered pellets before irradiation

Fig. 1 shows the microstructure of undoped and metal doped UO_2 pellets after sintering. Fig. 1(a)–(d) show the ceramographs for UO_2, 5%Mg–UO_2, 5%Mg–5%Nb–UO_2 and 3.5%Ti–UO_2, respectively, where a clear change by the metal oxide addition is seen. The grain size developed larger for 5%Mg–UO_2 and 3.5%Ti–UO_2 samples compared with undoped UO_2. The grain size of 3.5%Ti–UO_2 sample is outstandingly large. For 5%Mg–5%Nb–UO_2 pellet, the grain size is of the same order of magnitude as that of undoped UO_2 pellet but the grain edges were rounded while sintering.

The EPMA and SEM micrographs for the polished surface of 5%Mg–UO_2 pellet (20% enriched uranium) are displayed in Fig. 2. In the SEM micrograph shown in Fig. 2(b), the polygonal-shaped MgO particles of about 5 μm were precipitated in dispersion from the matrix. The MgO particles were also detected by EPMA (Fig. 2(a)). Since the MgO particles were still observed though not frequently for 2.5%Mg–UO_2, the solubility of magnesium in UO_2 is estimated to be slightly lower than 2.5 mol%. Such a low solubility is considered to be ascribed to the preparation method of the solid solution in this work. Usually, the solid solutions of high magnesium concentrations up to 10 mol% magnesium are produced by prolonged heating of the precursor solid solutions, which are formed in high oxygen partial pressure, in low oxygen partial presssure [26]. The simple method adopted here was for the sake of easy fabrication of the solid solutions.

The result of EPMA observation for 5%Mg–5%Nb–UO_2 is shown in Fig. 3. Both magnesium and niobium were precipitated along grain boundaries. Some oxide containing these elements melted on sintering at 1500°C. The eutectic compound of 27 mol% magnesium in $MgNb_9O_{24.17}$–$MgNb_2O_6$ having a melting point of 1430°C was likely to be formed [31].

The EPMA and SEM photographs for 3.5%Ti–UO_2 are shown in Fig. 4. The particles were grown up to exceedingly large sizes. Also, a compound containing titanium seems to have melted on heating. Titanium was detected along the grain boundaries by EPMA, resulting in densification as observed by the SEM micrographs (Figs. 4(b) and (c)).

The average grain sizes listed in Table 1 are a little differed in the samples of 10% and 20% enriched uranium, which would be due to the initial particle size and/or the variance in the pressure for pelletization since both the samples were sintered together under the same condition. The grain size of the undoped UO_2 sample was in the range 20–30 μm. These sizes are somewhat larger than those of standard type UO_2 fuel in current use [32]. For magnesium doped UO_2, the grain size increased with increasing concentration of magnesium. The grain size for 15%Mg–UO_2 sample was by about 2.5 times larger than that of undoped UO_2. Although the 5%Mg–5%Nb–UO_2 specimens heated at 1500°C for 0.5 h gave the average grain size essentially the same as those of undoped UO_2, it increased up to ~70 μm when the mixture was heated at a higher temperature of

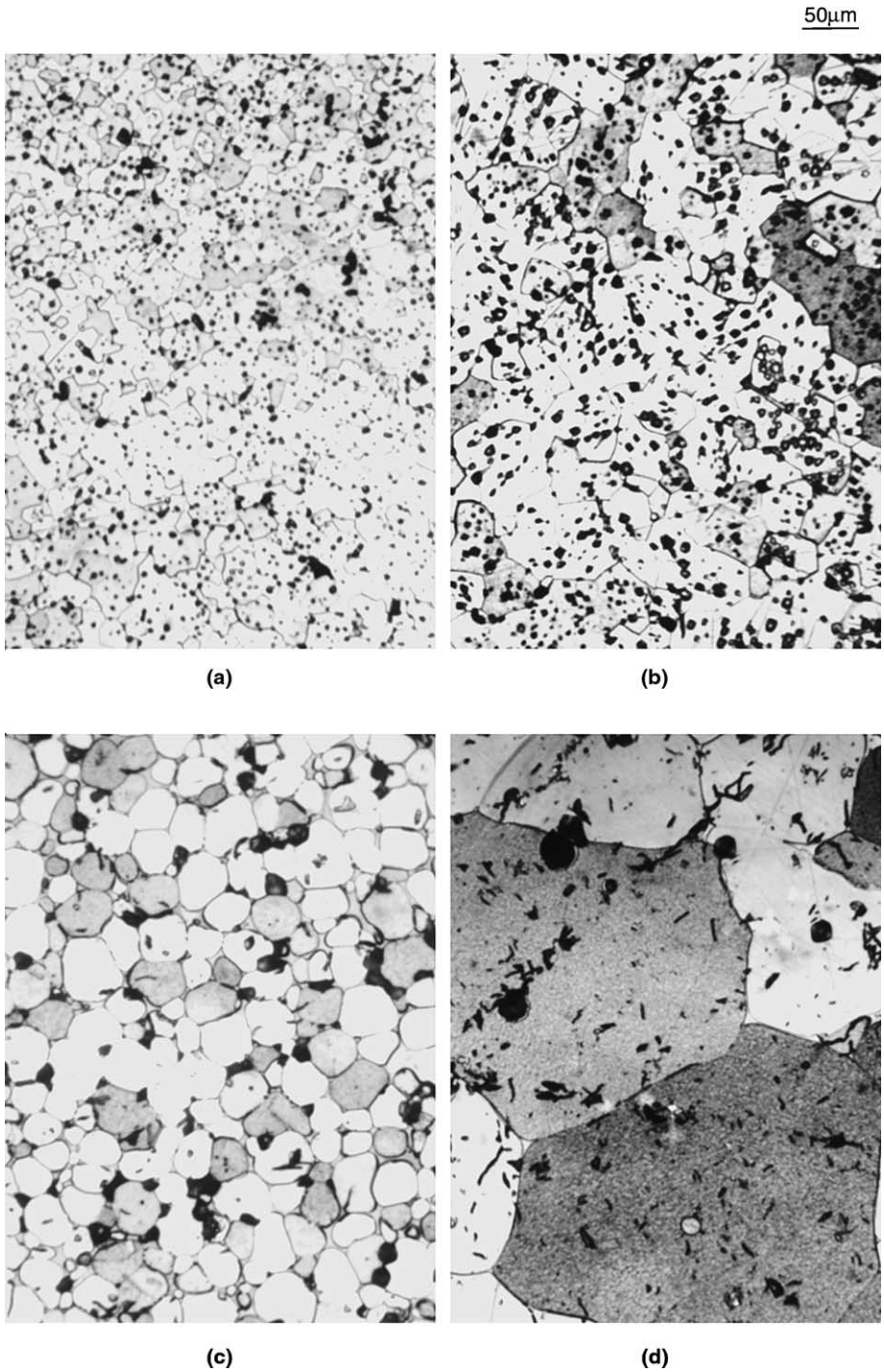

Fig. 1. Ceramographs for unirradiated sintered pellets: (a) undoped UO_2; (b) 5%Mg–UO_2; (c) 5%Mg–5%Nb–UO_2; (d) 3.5%Ti–UO_2.

1710°C for a longer period of 5 h. It is remarkable that the grain size of the 3.5%Ti–UO_2 specimen grew outstandingly large. The grain size attained 150 μm after sintering at 1550°C for 20 h. This reason has not been resolved unequivocally, but it is possible that the lower oxides of titanium, such as TiO, Ti_2O_3 and Ti_3O_5 having low melting points below 1700°C, reacted with UO_2 to yield some eutectic compounds [9,10,33].

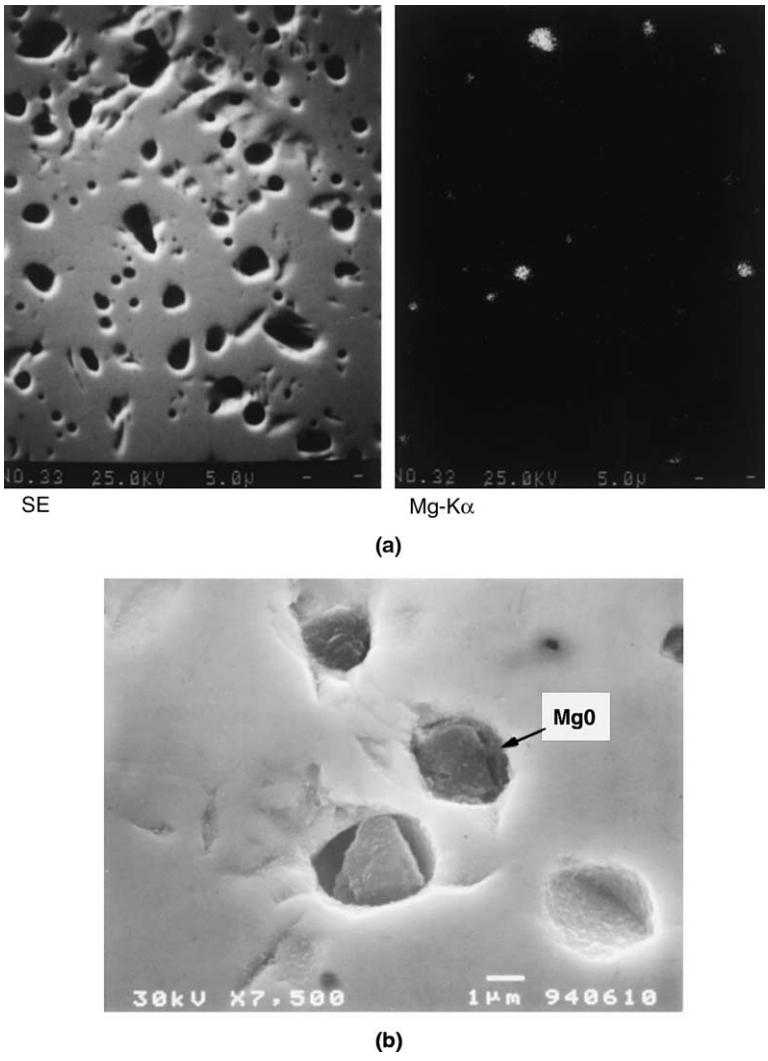

Fig. 2. EPMA and SEM micrographs for unirradiated sintered 5%Mg–UO_2 pellet (20% ^{235}U enrichment) on polished surface: (a) EPMA; (b) SEM micrograph.

The densities of the pellets measured by the fluid gravimetry method are listed in Table 2. It is characteristic of Mg–UO_2 specimens that their density decreased only slightly with increasing magnesium concentration in spite of the low atomic weight of magnesium. The percent of theoretical density, %TD, was calculated by assuming that the products were the mixtures of MgO and stoichiometric UO_2. As the lattice parameter of MgO, 4.2117 ± 0.0002 Å was used [34]. The %TD values were obtained as 95.5–96.8% for 2.5%Mg–UO_2, 97.3% for 5%Mg–UO_2, 97.5% for 10%Mg–UO_2 and 97.9–99.7% for 15%Mg–UO_2. This result shows that the %TD value increases with increasing magnesium content to near 100% at 15%Mg–UO_2. The above increase is considered to indicate the partial formation of the solid solution of interstitial magnesium type [35], rather than the enhancement of sintering by the addition of magnesium. To keep the %TD value 95–97%, the dissolved magnesium concentration in UO_2 becomes around 2 mol% which is in accord with the EPMA result.

4. Irradiation experiment

Irradiation of the sample pellets was carried out in a BRF-13H capsule in JRR-3M of Japan Atomic Energy Research Institute. As shown in Fig. 5, the cylindrical block made of Mo (27 mm diameter and 330 mm length) has three channels for inner capsules (fuel pins). The upper and middle sections of the block are designed for irradiation at lower temperature, and the lower section

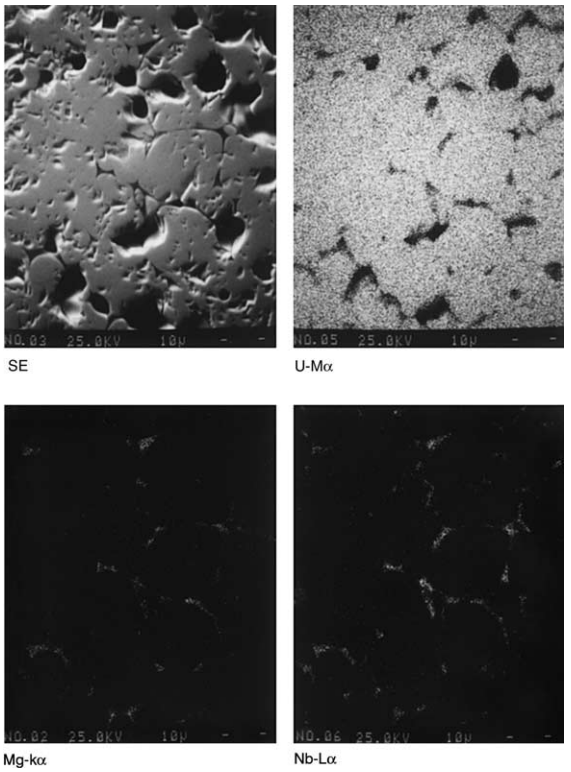

Fig. 3. EPMA photographs of 5%Mg–5%Nb–UO_2 (20% ^{235}U enrichment) on polished surface.

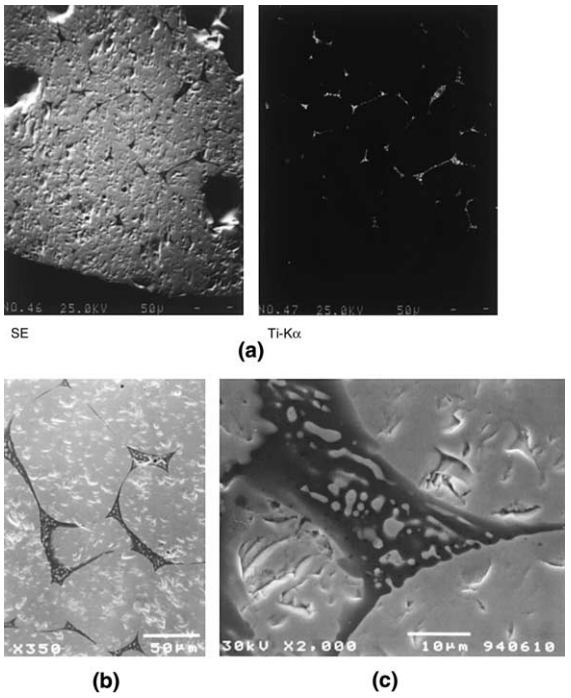

Fig. 4. EPMA and SEM micrographs for unirradiated sintered 3.5%Ti–UO_2 pellet on polished surface: (a) EPMA; (b) SEM; (c) higher magnification micrograph of (b).

for irradiation at higher temperature. In one channel, three fuel pins are set in series. The fuel pin consists of 1%Zr–Nb cladding with the dimensions of 8 mm∅ and 109 mm length. Each sample pellet was kept in a small Mo vessel with Mo lid. In a fuel pin, 17 such vessels are contained in an atmosphere of 0.1 MPa 5%Ar–He. The Mo block, which was contained in the middle capsule, was designed to play a role to raise and keep the temperature of the samples to high intended values by γ-heating as well as to minimize its change during long irradiation time. The irradiation temperature was controlled by changing the mixing ratio of He and N_2 gases filled in the gap between the middle and outer capsules. The Mo block is sealed in the middle capsule. The gap width was wider at the lower section so that the temperature of this section became higher on irradiation. The temperature was monitored by five thermocouples attached to the surface of the selected fuel pins.

The samples were irradiated for 257 days in 11 reactor cycles. The monitored temperatures during the above whole period are shown in Fig. 6. The highest temperatures were obtained at lower section (lines 1

Table 1
Grain size measured for the samples before irradiation

Sample	Average grain size (μm)	
	10% Enriched U	20% Enriched U
Undoped UO_2[a]	30	20
2.5%Mg–UO_2[a]	47	28
5%Mg–UO_2[a]	50	31
15%Mg–UO_2[a]	71	50
5%Mg–5%Nb–UO_2[b]	26 (71)[a]	26 (68)[a]
3.5%Ti–UO_2[c]	–	∼150

[a] 1710°C, 5 h in 4%H_2–He.
[b] 1500°C, 0.5 h in 4%H_2–He.
[c] 1550°C, 20 h in 4%H_2–He.

Table 2
Density of sintered pellets before irradiation

Sample	Density (g/cm^3)		
	6% Enriched U	10% Enriched U	20% Enriched U
Undoped UO_2	10.54	10.51	10.32
2.5%Mg–UO_2	–	10.52	10.38
5%Mg–UO_2	–	10.49	–
10%Mg–UO_2	10.34	–	–
15%Mg–UO_2	10.38	10.19	–

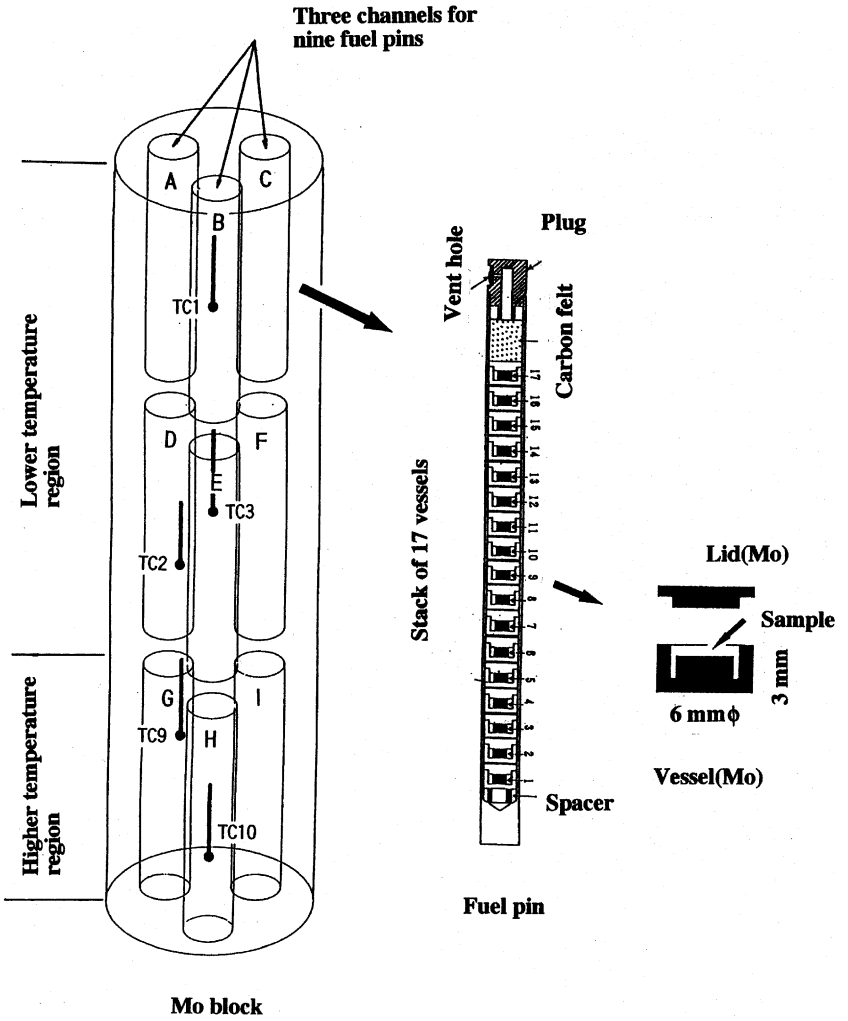

Fig. 5. Schematic drawing of BRF-13H capsule, fuel pin and fuel vessel used for irradiation.

and 2 in Fig. 6). Lines 3, 4, 5 and 6 show the monitored temperatures in the middle range 400–600°C. The temperatures of the middle capsule were monitored by two additional thermocouples attached to the outer surface of the capsule. Line 7 for the outer surface of the middle section was very low about 140°C. From lines 1 and 2 for the highest temperatures, the temperature is seen to decrease with irradiation time in each cycle. This lowering is mainly because of the heat from the enriched fuel pellets, of which the burnup increases rapidly with irradiation time. To overcome this lowering, the gas in the gap was changed from He having high thermal conductivity to low conductive N_2. As shown in Fig. 6, the temperature was recovered by this treatment. The effect of heat from the enriched fuel became much smaller after a few cycles of irradiation due to burnup.

The heat generated from a fuel pellet of maximum burnup, 91 GWd/tU, is estimated to be about 25 W, giving 190 W/cm linear heat rate at its earlier stage of irradiation. The linear heat rate of Mo γ-heating attained 280 W/cm by assuming the heat generation to be 3.2 W/g-Mo at the present irradiation hole. The inner temperatures could be estimated by reactor physical and heat conduction calculations using the modified GENGTC code [36]. The calculated results for 175–186 W/cm linear heat rate of the fuel with 50%He–50%N_2 gap gas showed that the inner surface of the fuel pin cladding was higher than the outer surface, at which the temperature was monitored, of 600°C by 10° (upper section) and that the difference was smaller, i.e. 5° if the outer surface was 1000°C (lower section). The pellet temperature was higher than that of the outer surface by 100°C at the radial periphery of the pellets. This difference did

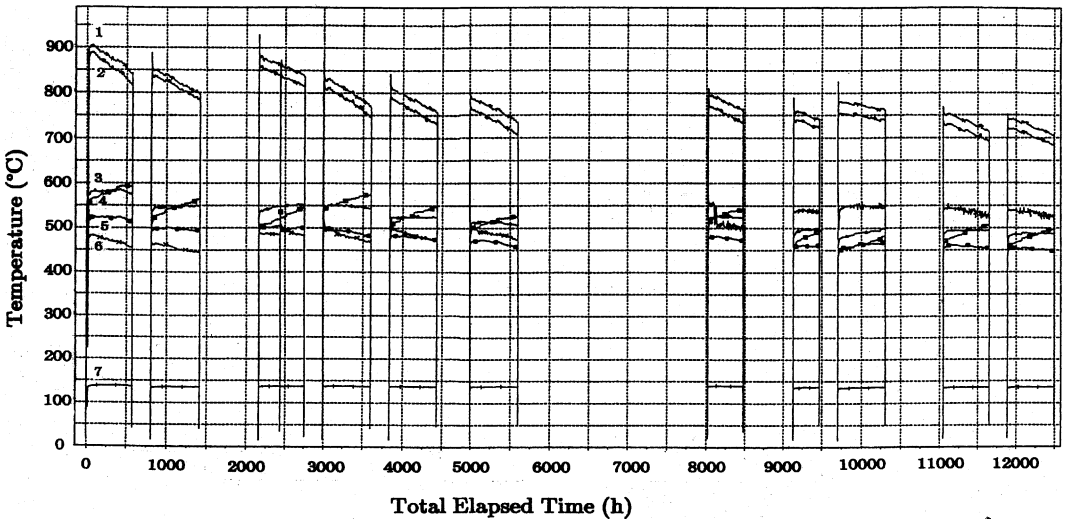

Fig. 6. Monitored temperatures on irraditation as a function of total elapsed time. Line 1: Lower part of lower section; Line 2: Upper part of lower section; Line 3: Upper part of middle section; Line 4: Middle part of upper section; Line 5: Lower part of middle section; Line 6: Outer surface of middle capsule at lower section; Line 7: Outer surface of middle capsule at middle section.

not change with section (namely temperature). At the central part of the fuel pellets, the temperature was higher than that of rim part but only by 4–5°. From these values, the 100°C criterion for temperature correction was derived.

The corrected temperature was 600–700°C in the lower temperature region at the early stage of irradiation. It lowered below 650°C thereafter. The corrected temperature was 900–1000°C in the higher temperature region at first, and then it lowered slowly below 930°C. From the temperature distribution obtained by extrapolation and/or interpolation of the temperatures of the measured points, the irradiation temperature of each oxide pellet was estimated. For considering the accuracy of the fuel temperatures, the mixing ratio of the gap gas in the criterion needs to be taken into account. However, calculation shows that the mixing ratio does not cause a large change in temperature. The error in the corrected fuel temperatures is estimated to be within ±50°C.

Three couples of fluence monitors for fast and thermal neutrons were instrumented at the upper, middle and lower sections between the Mo block and the middle capsule. For fast and thermal neutrons, ^{54}Fe and ^{59}Co wires were used, respectively, for which activation analysis was carried out after irradiation. The highest fluence was observed for the pins in the middle section. The fluences for fast and thermal neutrons were 8.8×10^{20} and 1.7×10^{21} n/cm^2, respectively. The lowest fluence was observed for the fuel pins in the lower section where fast and thermal neutrons were 0.6×10^{20} and 0.7×10^{21} n/cm^2, respectively.

5. Post-irradiation examinations

5.1. Burnup

The burnup of the oxide specimens was determined using the pulse height analysis data for the γ-activities of ^{137}Cs and ^{144}Ce measured after three months of cooling. First, the migration of these elements during irradiation was checked by axial γ-scanning of the fuel pins. For the fuel pins irradiated at lower temperatures of 550–650°C (pins A–F of Fig. 5), most of the ^{137}Cs was found to be kept maintained in the UO_2 matrix though a small amount of ^{137}Cs moved to the upper plenum of the pin. ^{144}Ce was well held in the UO_2 matrix. For the fuel pins irradiated at higher temperatures of 800–930°C (pins G–I), most of the ^{144}Ce still remained in the UO_2 matrix, but a significant ratio of ^{137}Cs was found to migrate to the upper plenum. On this basis, the burnup of the fuel was calculated by the use of the ^{137}Cs and ^{144}Ce data from the fission yield of these isotopes after a careful correction for the ^{137}Cs migration. The pulse height analysis was carried out for 12 sample pellets taken out from the fuel pins. The burnups attained during the irradiation period were 35, 62 and 94 GWd/tU (max) for the samples of 6%, 10% and 20% enriched uranium, respectively.

5.2. Observation of irradiated samples

Irradiated pellets were first examined by a microscope of low magnifications. The results are shown in Table 3. The position of the samples with numbers 1–17 in each fuel pin is illustrated in Fig. 5. It is seen from the

Table 3
Visual observation of irradiated samples

Capsule		Upper Section			Middle Section			Lower Section			Number of Samples
Burnup (GWd/t)	20 %eU 6 & 10% eU	84 - 87 32 - 34 , 60 - 62			85 - 94 34 - 35 , 51 - 55			60 - 66 19 - 21 , 32 - 34			
Temperature (℃)		550 - 640			560 - 650			800 - 930			
Sample＼Fuel Pin		A	B	C	D	E	F	G	H	I	
20 %eU	3.5%Ti	⑰＊	⑰△	⑰＊	⑰＊	⑰＊	⑰＊	⑰＊	⑰＊	⑰＊	34
		⑯＊	⑯＊	⑯＊	⑯＊	⑯＊	⑯＊	⑯＊	⑯＊	⑯＊	
		⑮＊	⑮＊	⑮＊	⑮＊	⑮＊	⑮△	⑮＊	⑮＊	⑮＊	
				⑭＊			⑭＊		⑭＊	⑭＊	
				⑬＊						⑬＊	
										⑫＊	
	5%Mg-5%Nb	⑭△		⑫△	⑭△	⑭△		⑭△			5
	15%Mg		⑭△	⑪△			⑬△			⑪＊	6
							⑫＊			⑩＊	
	5%Mg		⑬△			⑬＊			⑬＊		6
			⑫△			⑫＊			⑫＊		
	2.5%Mg	⑬＊			⑬＊			⑬＊			6
		⑫＊			⑫△			⑫＊			
	Undoped	⑪＊	⑪＊	⑩△	⑪△	⑪△	⑪△	⑪＊	⑪＊	⑨＊	38
		⑩△	⑩△	⑨△	⑩△	⑩△	⑩△	⑩＊	⑩＊	⑧＊	
		⑨＊	⑨△	⑧＊	⑨△	⑨△	⑨△	⑨＊	⑨＊	⑦＊	
		⑧＊		⑦△	⑧△	⑧△	⑧△	⑧＊	⑧＊	⑥＊	
				⑥△			⑦△		⑦＊		
10 %eU	5%Mg-5%Nb	⑦◎	⑧◎		⑦◎		⑥△	⑦＊			5
	15%Mg	⑥◎	⑦◎		⑥◎	⑦◎		⑥◎			6
								⑤◎			
	5%Mg			⑤△			⑤◎			⑤◎	6
				④△			④◎			④◎	
	2.5%Mg		⑥△			⑥◎			⑥◎		6
			⑤◎			⑤◎			⑤△		
	Undoped	⑤◎			⑤◎			④◎			6
		④◎			④◎			③◎			
6 %eU	5%Mg-5%Nb	③◎		③◎	③◎		③◎			③＊	5
	15%Mg		④◎			④◎			④◎		6
			③◎			③◎			③◎		
	10%Mg			②◎			②◎			②◎	6
				①◎			①◎			①◎	
	2.5%Mg		②◎			②◎			②◎		6
			①◎			①◎			①◎		
	Undoped	②◎			②◎			②◎			6
		①◎			①◎			①◎			

①～⑰ : Sample No. ;

◎ : Intact ; △ : Cracked ; ＊ : Heavily Fragmented .

table that all the irradiated pellets of 20% enrichment (95 specimens out of 153 specimens) were cracked regardless of metal doping or not. The 3.5%Ti–UO_2 samples were especially heavily damaged. They were fractured into fine pieces. The burnups of the fuel oxides with 20% ^{235}U enrichment were above 60 GWd/tU. It is worth noting that in this work each pellet was separately set in the Mo vessel under the condition free from mechanical restraint of the cladding unlike the LWR fuels of closed gap and also in the low pressure of 5%Ar–He gas (2–3 atm at irradiation temperature). The pellet dimensions were of 3 mm$\varnothing$ and 1 mm thicknesses. Namely, the pellets were much smaller than the LWR pellets. The fuel temperature was very quickly changed when an irradiation cycle was starting or stopping.

Therefore, the high burnup state of LWR fuels cannot be discussed directly only from the present data. However, information obtained from Table 3 is important and meaningful. A point which can be marked is that the burnup of the fuels of 20% ^{235}U enrichment in the lower section (higher temperature region) was 60–66 GWd/tU which is virtually the same as the burnup (60–62 GWd/tU) of the fuels of 10% enrichment in the upper section (lower temperature region with 550–640°C). All the samples were cracked or fragmented under the former condition, but about 70% of the samples were intact under the latter condition. The cracked pellets were two for 10% enriched 5%Mg–UO_2 and one for 2.5%Mg–UO_2. However, all 15%Mg–UO_2 pellets were intact, suggesting that there is a possibility of increased resistance against cracking for magnesium doped pellets. The result shows that the important factor affecting the shape integrity of the pellet should be the thermal stress at startup and shutdown of reactor: The fuel oxides of 60 GWd/tU burnup may be cracked if the temperature is high (800–930°C) and therefore thermal

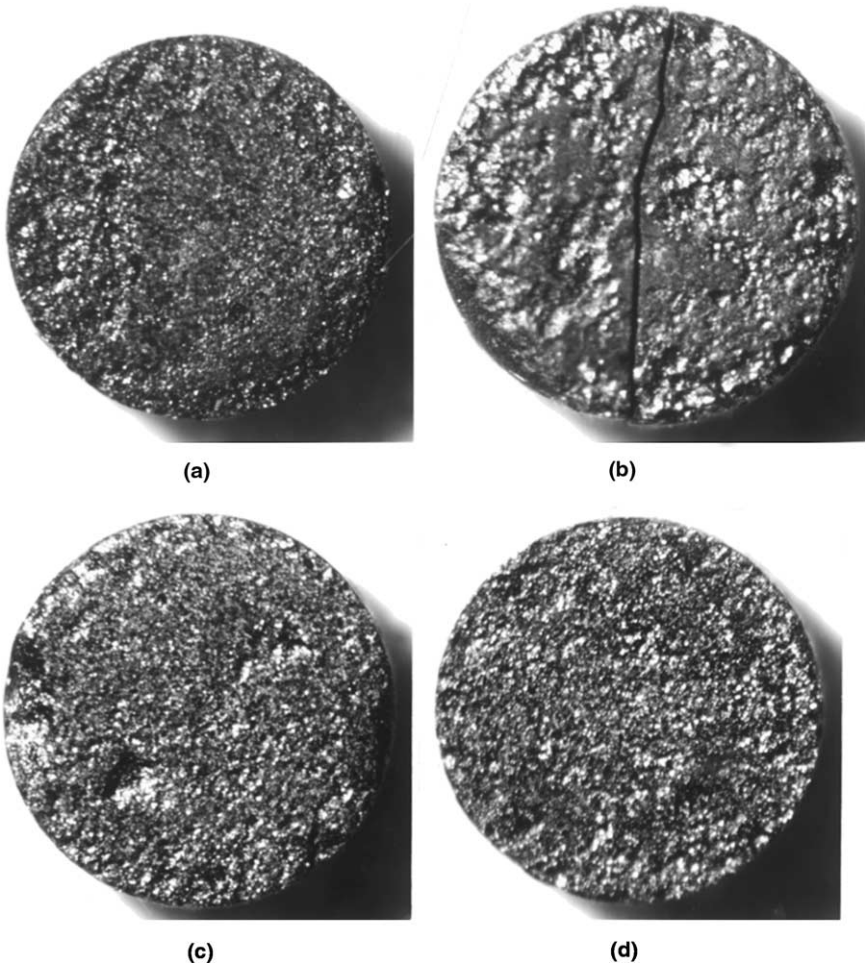

Fig. 7. Appearance of irradiated pellets: (a) undoped UO_2 (G-1) irradiated to 19 GWd/tU at 800–900°C; (b) undoped UO_2 (E-8) irradiated to 91 GWd/tU at 560–600°C; (c) 5%Mg–UO_2 (F-4) irradiated to 53 GWd/tU at 560–600°C; (d) 15%Mg–UO_2 (A-6) irradiated to 61 GWd/tU at 550–640°C.

Table 4
Swelling of undoped and Mg doped UO_2 pellets after irradiation

Sample	Enrichment (%)	Burnup (GWd/tU)	Irradiation temp. (°C)	Density (g/cm^3)	Swelling ($\Delta V/V \times 100$)
Undoped UO_2	6	19–20	800–900	10.48	0.64
		34	550–640	10.57	0.0
		34-35	560–600	10.36	1.71
Undoped UO_2	10	60	550–640	10.40	1.04
Undoped UO_2	20	87–94	560–600	9.02	14.40
2.5%Mg–UO_2	10	53	560–600	10.26	2.55
		60–62	550–640	10.14	3.73
5%Mg–UO_2	10	32–33	800–900	10.23	2.56
		53–54	560–600	10.06	4.25
10%Mg–UO_2	6	19–20	800–900	10.27	0.70
		34	550–640	10.20	1.36
		34	560–600	10.10	2.36
15%Mg–UO_2	6	21	800–900	10.11	2.63
		33–34	550–640	10.21	1.64
		35	560–600	10.13	2.44

shock is large. The steep temperature change is depicted in Fig. 6.

The burnups of the 10% enriched samples were 60–62, 51–55 and 32–34 GWd/tU in the upper section (550–640°C), middle section (560–650°C) and lower section (800–930°C), respectively. At this enrichment, the samples were mostly intact. But one 5%Mg–5%Nb–UO_2 pellet irradiated at higher temperatures of 800–930°C was fragmented into many pieces. The burnups of the 6% enriched samples were 32–34, 34–35 and 19–21 GWd/tU in the upper, middle and lower sections, respectively. For these low enriched fuels, all samples were intact except for 5%Mg–5%Nb–UO_2 irradiated at the higher temperature of 800–930°C. It seems likely that the 5%Mg–5%Nb–UO_2 pellet is unstable to thermal shock at high temperatures under irradiation.

In Fig. 7, the integrity of the irradiated pellets is exemplified. The coarse surface seen for the pellets is because all pellets were irradiated as they were without polishing. The upper left is the appearance of the undoped UO_2 pellet irradiated to 19 GWd/tU in the high temperature region of 800–930°C. No crack was formed in the pellet. The upper right shows the appearance of the undoped UO_2 pellet highly irradiated to 91 GWd/tU at 560–650°C. Here a large crack running through the pellet is seen. The lower left shows the 5%Mg–UO_2 sample irradiated to 53 GWd/tU at 560–650°C, and the lower right the 15%Mg–UO_2 sample irradiated to 61 GWd/tU at 550–640°C. These two samples were intact after irradiation.

5.3. Swelling

The swelling of pellets by irradiation is demonstrated for undoped UO_2 and magnesium doped UO_2. For this purpose, the densities of the irradiated pellets were measured by the fluid gravimetry method. The swelling rate was calculated by dividing the difference of the densities before and after irradiation by the density before irradiation. As the density before irradiation, one representable value was used for the samples of one kind. The densities listed in Table 2 were used as the adoptable values before irradiation.

The obtained swelling rates in percent were listed in Table 4, and plotted as a function of burnup in Fig. 8,

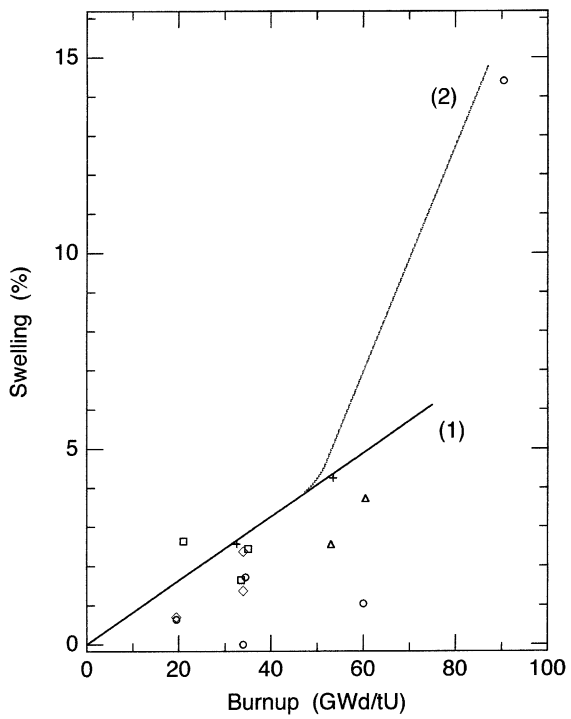

Fig. 8. Swelling of irradiated pellets as a function of burnup: (○) undoped UO_2; (△) 2.5%Mg–UO_2; (+) 5%Mg–UO_2; (◇) 10%Mg–UO_2; (□) 15%Mg–UO_2.

in which the possible densification at lower burnups below 5–10 GWd/tU is implicitly included. Since the samples used in this work had the grain size same as or larger than ~30 μm, the densification is estimated to be very small, viz. <0.2%. It was practically unable to measure the density of finely fragmented samples, so that the acquisition of the swelling data was made for the samples which were intact or cracked into large two or several pieces with the burnup below ~60 GWd/tU.

Fig. 8 indicates that the swelling increases with increasing burnup, but it can be regarded that the swelling rate is lower than 4% at burnups below 60 GWd/tU. The largest swelling observed below 60 GWd/tU was 4.3% shown by the 5%Mg–UO_2 sample of 53–54 GWd/tU burnup at 560–600°C. Because the number of data was not large and the measured values scattered, it is difficult to have any definitive conclusion with regard to the swelling for undoped UO_2 and Mg–UO_2. But there seems to be no significant difference between the swelling rate of undoped UO_2 and Mg–UO_2. The apparent change is in a range of fluctuations of the swelling rate caused by larger errors which were produced on measuring the densities two times, i.e. before and after irradiation. The solid straight line (line 1) in the figure is the literature value for undoped UO_2 of 96% TD, showing the swelling rate to be 0.081% per GWd/tU burnup [37]. The most present data are below this line. The swelling for 15%Mg–UO_2 of 21 GWd/tU is above this line, but its irradiation temperature was high (800–900°C). According to [38], the pellets swell at the rate of 0.1% per GWd/tU up to 70 GWd/tU.

The dotted line for the burnup above 50 GWd/tU has a slope 0.31% per GWd/tU burnup [37]. Such a high swelling rate is considered to be associated with the rim structure which emerges at high burnups. For the undoped UO_2 sample with a high burnup of about 90 GWd/tU (560–600°C), which was cracked but not fragmented to small pieces, the present measurement gave the swelling of 14.4%. The measured sample exhibited the rim structure all over the surface. The above swelling is well in accord with the literature dotted line. However, a swelling rate of 0.15% per GWd/tU has also been reported for a PWR fuel with centerline temperatures around 1000°C at a burnup of 102 GWd/tU [39]. For this fuel disk, the formation of extended rim structure was noticed over a distance of 1.15 mm to about $r/r_0 = 0.75$, where r is the distance from the pellet center and r_0 the radius. The latter swelling rate is smaller probably due to non-uniformity of the rim structure in the pellet.

5.4. Thermal conductivity

The effect of the surface polishing on the thermal diffusivity measurement was studied for two kinds of unirradiated undoped UO_2 pellets, namely the pellets of unpolished surfaces and those of polished surfaces. The result showed no difference in the thermal diffusivities of these samples. Then, the thermal diffusivities of irradiated samples were measured without polishing. The measured samples were undoped UO_2, 5%Mg–UO_2 and 15%Mg–UO_2. The thermal diffusivity measurements were carried out before and after irradiation for these samples. The burnups of the undoped UO_2, 5%Mg–UO_2 and 15%Mg–UO_2 samples were 60 GWd/tU (550–640°C), 32 GWd/tU (800–900°C) and 35 GWd/tU (560–600°C), respectively.

From the measured thermal diffusivities, the thermal conductivity was calculated by the relation

$$\lambda = \alpha \rho C_p, \tag{1}$$

where λ, α, ρ and C_p are the thermal conductivity, thermal diffusivity, the bulk density and the specific heat of the sample, respectively. The room temperature densities of the unirradiated and irradiated samples were those obtained by fluid gravimetry measurements. The densities at higher temperatures were calculated using the reference data of the linear thermal expansion coefficient for UO_2 [40]. No correction was made for the change of thermal expansion due to MgO addition, since the linear thermal expansion coefficient of MgO was close to that of UO_2 (1.6% at 1400°C) [41]. The specific heat capacities of Mg–UO_2 were approximated from the reference values for MgO and UO_2 [42] according to Kopp's law as

$$C_p(Mg_yU_{1-y}O_{2-y}) = yC_p(MgO) + (1-y)C_p(UO_2). \tag{2}$$

In Fig. 9, the thermal conductivities are plotted against temperature. As a literature curve, the thermal conductivity change of the unirradiated undoped UO_2 of 95% theoretical density is shown as the dash–dotted line [43]. As seen from the figure, the unirradiated undoped UO_2 sample with 96% TD gives higher thermal conductivities than the literature values. In the present samples, Mg–UO_2 showed higher thermal conductivities than undoped UO_2. The thermal conductivity increased with increasing concentration of magnesium. This increase is considered to be because the Mg–UO_2 samples were largely composed of the mixture of MgO and UO_2 and the thermal conductivity of MgO is higher than that of UO_2 [44].

As for the irradiated specimens, the thermal conductivities of the undoped UO_2 pellet of 60 GWd/tU burnup with a bulk density of 10.40 g/cm^3 (95% TD) are shown by ○ marks and solid line in Fig. 9. By irradiation, the conductivity is seen to be much lowered. The conductivity drop was especially conspicuous at lower temperatures, viz. 3.5 Wm^{-1} K^{-1} at 450 K, which is known as the results of formation of the high concentration of defects and fission products together with lattice deformations caused by irradiation. The curve (1st run) is in good agreement with that of the first measurement run by Nakamura et al. [45] for the und-

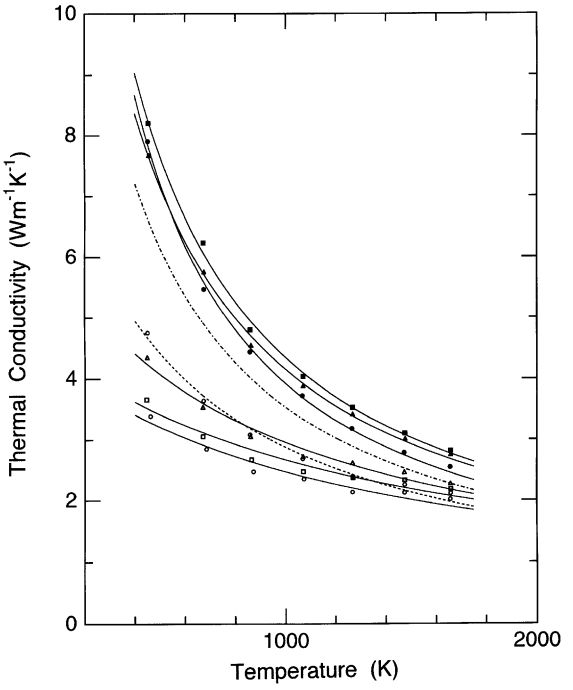

Fig. 9. Change of thermal conductivity with temperature: (—●—) unirradiated undoped UO_2 (95.9% TD); (—○—) irradiated undoped UO_2 (60 GWd/tU, 1st measurement); (··○··) irradiated undoped UO_2 (2nd measurement); (—▲—) unirradiated 5%Mg–UO_2 ($d = 10.49$ g/cm^3); (—△—) irradiated 5%Mg–UO_2 (32 GWd/tU); (—■—) unirradiated 15%Mg–UO_2 ($d = 10.38$ g/cm^3); (—□—) irradiated 15%Mg–UO_2 (35 GWd/tU); (—·—·—) reference curve for 95% TD unirradiated undoped UO_2 [43].

oped UO_2 samples irradiated up to 63 GWd/tU in the whole temperature range from 200°C to 1400°C. Agreement is also good with the reported thermal conductivities of UO_2 irradiated to 40 GWd/tU [46].

The thermal conductivity is reported to recover if defects are annealed during thermal diffusivity measurement at high temperatures [47]. Then, the measurement was repeated again in the temperature range from 200°C to 1400°C for the undoped UO_2 sample of which the thermal diffusivity had once been measured. The result is shown by the combination of ○ marks and broken line (2nd measurement) in Fig. 9. The thermal conductivity is clearly recovered from the first measurement. The value at 450°C, for example, increased to 4.8 Wm^{-1} K^{-1}. The data on thermal conductivity recovery by thermal annealing are rather sparse. Recently Yagnik [46] reported that the thermal conductivity almost completely recovered after several times of repeated measurements up to 1500°C. The present thermal conductivities are consistent with those of Yagnik though the recovery rate is somewhat faster in our measurements. With regard to the recovery rate, the time to keep at high temperatures for thermal diffusivity measurement may be related.

The thermal conductivities of irradiated samples of 5%Mg–UO_2 and 15%Mg–UO_2 are shown in Fig. 9 by △ and □ marks, respectively. Their burnups of 32 and 35 GWd/tU were about half of that of the undoped UO_2 sample measured in this work. The repeated measurements to study the annealing effect were not performed for these irradiated Mg–UO_2 samples. Due to perhaps the lower burnup of Mg–UO_2 samples, the irradiated 5%Mg–UO_2 and 15%Mg–UO_2 pellets exhibited fairly higher thermal conductivities than the undoped UO_2 sample of 60 GWd/tU burnup (1st measurement). The thermal conductivities of the irradiated 15%Mg–UO_2 pellet, of which the density was 10.13 g/cm^3, were 3.7 and 2.1 W m^{-1} K^{-1} at 450 and 1660 K, respectively. Fig. 9 shows that the thermal conductivities of 15%Mg–UO_2 are higher than those of 5%Mg–UO_2 for unirradiated samples, while this order is reversed for irradiated samples. It may be the case that the fuel which contains high concentrations of foreign metal is more susceptible to atomic scale damage in the crystal during irradiation. All the irradiated specimens of undoped UO_2 (1st measurement), undoped UO_2 (2nd measurement), 5%Mg–UO_2 and 15%Mg–UO_2 give the thermal conductivities approaching closer to the values of 2.0–2.3 Wm^{-1} K^{-1} at higher temperatures above 1500 K. The relatively large difference in the thermal conductivities of the unirradiated and irradiated samples which remained still at high temperatures has been explained as due to the change in the constituting elements by fission and insufficient thermal annealing of the defects [47].

The curves in Fig. 9 are those obtained by fitting with the least-squares calculations to the following expression of thermal conductivity, λ, on the basis of phonon scattering mechanism [49,50],

$$\lambda = \frac{1}{A + BT}, \tag{3}$$

where A and B are the constants and T is the absolute temperature. The fitted lines well follow the experimental points of Fig. 9, showing that the thermal conductance is essentially of the phonon scattering type for the present fuel oxides. The calculated A and B values of Eq. (3) are listed in Table 5. It is seen that the A value (temperature independent term) was largely increased by irradiation, in contrast to the B value which was slightly decreased. The change of the A and B values was approximated by

$$A = 2.5 \times 10^{-2} + 2.5 \times 10^{-3} \cdot \mathrm{BP} + 7.7 \times 10^{-3} \cdot \mathrm{BP}(y + 8.8 \times 10^{-3})^{1/2}, \tag{4}$$

and

$$B = 2.32 \times 10^{-4} - 7.7 \times 10^{-7} \cdot \mathrm{BP} - 2.2 \times 10^{-4} y, \tag{5}$$

Table 5
A and B values for thermal conductivity λ expressed as $\lambda = 1/(A + BT)$ (W m^{-1} K^{-1})

Sample	Burnup (GWd/tU)	A (m K/W)	B (m/W)
Undoped UO_2	–	2.268×10^{-2}	2.320×10^{-4}
Undoped UO_2 (1st measurement)	60	2.183×10^{-1}	1.854×10^{-4}
Undoped UO_2 (2nd measurement)	60	1.057×10^{-1}	2.414×10^{-4}
5%Mg–UO_2	–	3.897×10^{-2}	2.016×10^{-4}
5%Mg–UO_2	32	1.532×10^{-1}	1.845×10^{-4}
15%Mg–UO_2	–	3.115×10^{-2}	1.989×10^{-4}
15%Mg–UO_2	35	2.098×10^{-1}	1.643×10^{-4}
Ref. [43]	–	4.325×10^{-2}	2.389×10^{-4}

where BP is the burnup in GWd/tU and y is the magnesium concentration in the $Mg_yU_{1-y}O_{2-y}$ formula (even if the sample is the mixture of MgO and UO_2). The linear dependence of A and B on BP has been supported experimentally [48]. The decrease of the thermal conductivity by irradiation is mainly attributable to the increase of the temperature independent term, A. Since this term has the property related to the concentration of defects and impurity species that hinder the harmonicity of lattice vibrations, its increase with irradiation is well understood. On the other hand, the phonon mean free path is proportional to $1/T$ at high temperatures. The B term is the proportionality constant which does not change greatly with irradiation.

5.5. Fuel microstructures

5.5.1. Undoped UO_2

The SEM micrographs of unirradiated UO_2 and irradiated UO_2 (51 GWd/tU, 560–600°C) are shown in Figs. 10(a) and (b), respectively. The irradiated pellet was intact and showed that the pores did not largely change from those of the unirradiated pellet, though the grain subdivision was in a way to develop with bubbles, which is regarded as one of the preceding phenomena before the formation of the rim structure starting from the pellet periphery of high burnup LWR fuels [51–53]. In this irradiated pellet, the rim structure was not formed.

The samples irradiated to high burnup (87–94 GWd/tU) in the lower temperature region (560–600°C) were fractured to large pieces. In their fractured faces, sharp edges were frequently observed, which suggests that the thermal stress at startup and shutdown of the reactor during irradiation is responsible for the pellet breakage. Fig. 11(a) shows the fragments of pellets D-9, 10 and E-9, 10. In the SEM micrographs shown in Figs. 11(b) and (c), the bubbles have coalesced forming intergranular pores leading to give sub-divided grains and the rim structures on the whole pellet surface. For the formation of the large bubbles, the relation of depression of xenon has been discussed. It has been reported that most of the missing matrix gas was not released to the rod free volume but was retained in the gas pores of the rim structure [54]. In the PWR fuel samples of 102 GWd/ tU burnup, some of the gas bubbles at the pellet rim were observed to have grown to almost 10 μm in size, which has been assumed to be a consequence of over-pressurization caused by the continuous accumulation of fission gas in the bubbles [39].

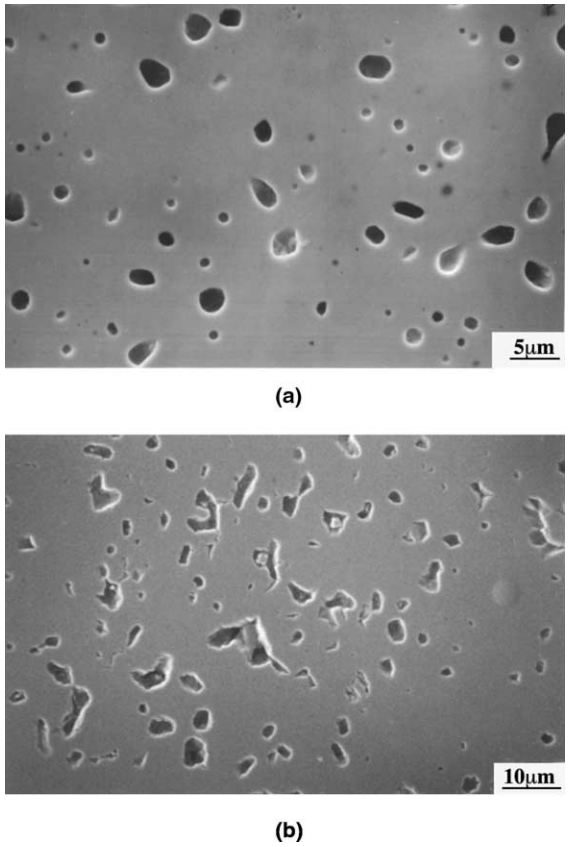

Fig. 10. SEM micrographs for undoped UO_2: (a) unirradiated UO_2 ($d = 10.51$ g/cm^3); (b) irradiated UO_2 (D-4, 51 GWd/tU, 560–600°C).

The sample pellet G-9 irradiated at high temperatures of 820–930°C was fractured into fine pieces already

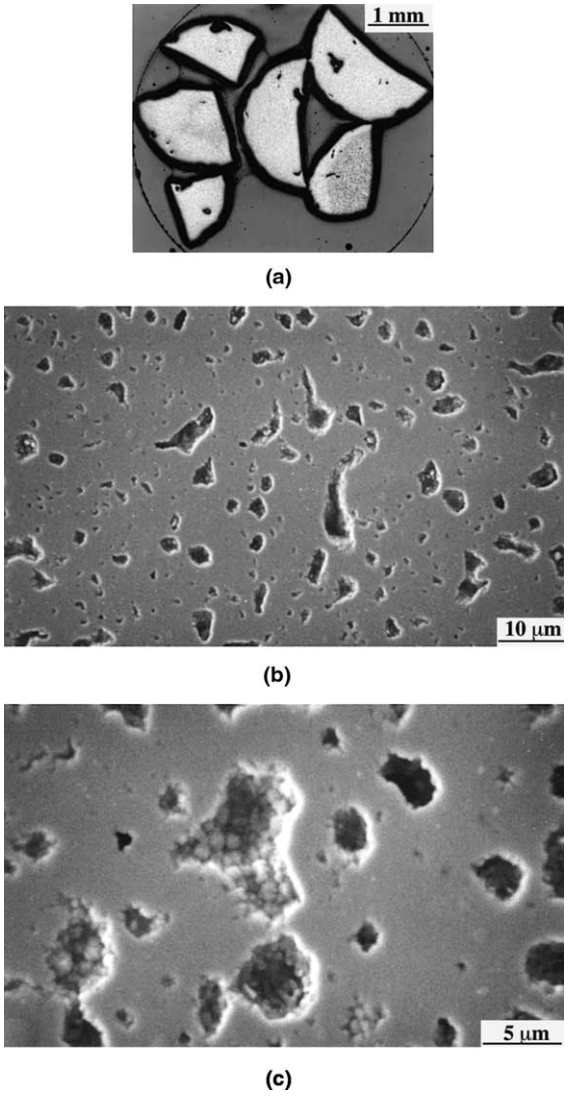

Fig. 11. High burnup irradiation of undoped UO_2: (a) fragments of D-9,10 and E-9,10 pellets (87–94 GWd/tU, 560–600°C); (b) SEM micrograph; (c) higher magnification SEM micrograph.

at 62 GWd/tU burnup (Fig. 12(a)). The straight fracture line and many sharp edges indicate that the fragmentation was caused by thermal stress. For this sample, the submicronic grain surfaces and the rim structures were not detected. As shown in the ceramograph of Fig. 12(b), there were white precipitates which consist of metallic Mo, Tc, Ru, Rh and Pd (Fig. 12(c)). The high irradiation temperature is assumed to induce the formation of the above metallic precipitates.

5.5.2. Magnesium doped UO_2

Figs. 13(a), (b) and (c) are the ceramograph, SEM micrograph and EPMA photograph, respectively, of

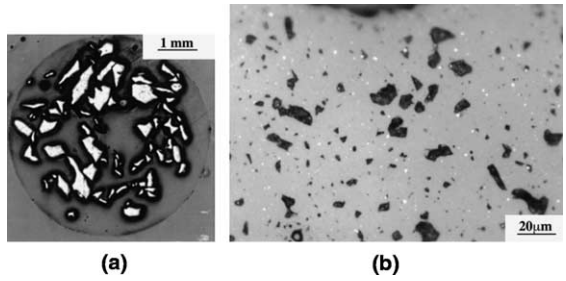

Fig. 12. High temperature irradiation of undoped UO_2: (a) fragments of G-9 pellet (62 GWd/tU, 820–930°C); (b) ceramograph showing white inclusions; (c) EPMA.

5%Mg–UO_2 sample (F-4) irradiated to 53 GWd/tU at 560–600°C. The pellet was almost intact (Fig. 13(a)), but the subgrain formation proceeded on the pore surfaces as can be seen in Fig. 13(b). However, the microstructure where the dispersed MgO remained to exist did not change in the EPMA photographs of Fig. 13(c). Figs. 14(a)–(c) are the photographs for high burnup 5%Mg–UO_2 (91 GWd/tU, 600–650°C). As shown in Fig. 14(a), the pellets fractured straight. Fig. 14(b) is a ceramograph of higher magnification. The surface structure of this specimen observed by EPMA is indicated in Fig. 14(c). In the large bubbles, the sub-divided grains can be observed. Magnesium is distributed uniformly in the UO_2 matrix. In the other part, the spot-like MgO particles were also found to exist. These micrographs show the partial dissolution of magnesium in UO_2. The solubility of magnesium would be around 2 mol% as described in the section where the sintered pellets were observed before irradiation.

The microstructures of the 15%Mg–UO_2 sample are shown in Fig. 15. Figs. 15(a) and (b) exhibit the etched structure ceramograph and the SEM micrograph of the unirradiated 15%Mg–UO_2 sample, respectively. Figs. 15(c)–(e) are the photographs for the irradiated A-6 sample (61 GWd/tU, 550–640°C). This pellet was intact after irradiation yielding a swelling of 2.3%. Fig. 15(c) shows the ceramograph of the fractured surface of an artificially broken pellet. Figs. 15(d) and (e) indicate the SEM micrograph and the EPMA result, respectively, showing the polished surface and dispersion of magnesium. The pores were wholly unchanged by irradiation, and the MgO-spot remained to exist. The first indication of subgrain formation was seen but no rim structures were detected to develop. The platinum-family metals were distributed homogeneously in the matrix without the formation of precipitates.

Figs. 16(a) and (b) show the ceramograph and EPMA photograph for F-13 high burnup 15%Mg–UO_2 specimen (91 GWd/tU, 600–650°C). The pellet was cracked straight (Fig. 16(a)). In the EPMA micrograph, the large bubbles were accompanied by the rim struc-

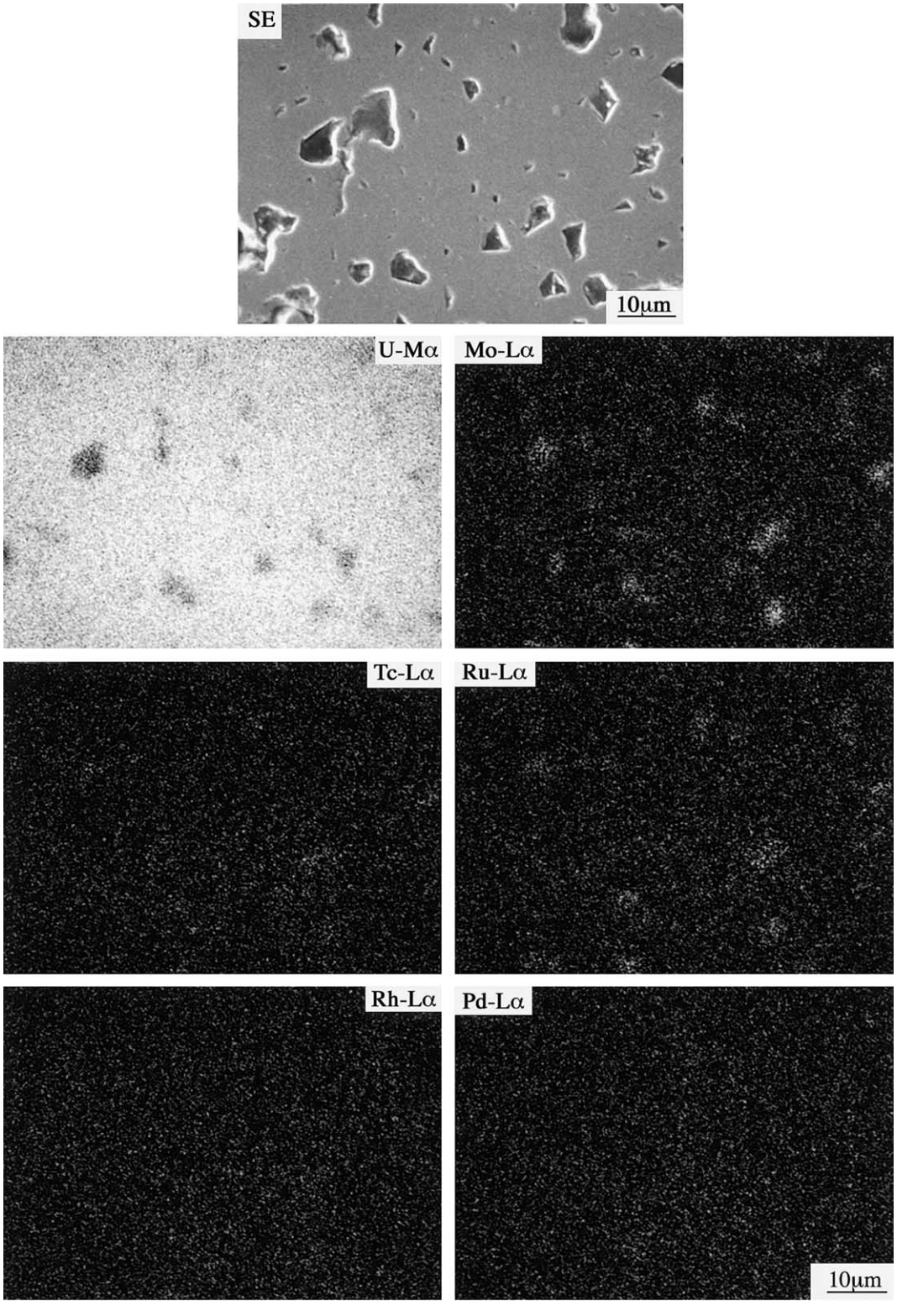

(c)

Fig. 12. (Continued).

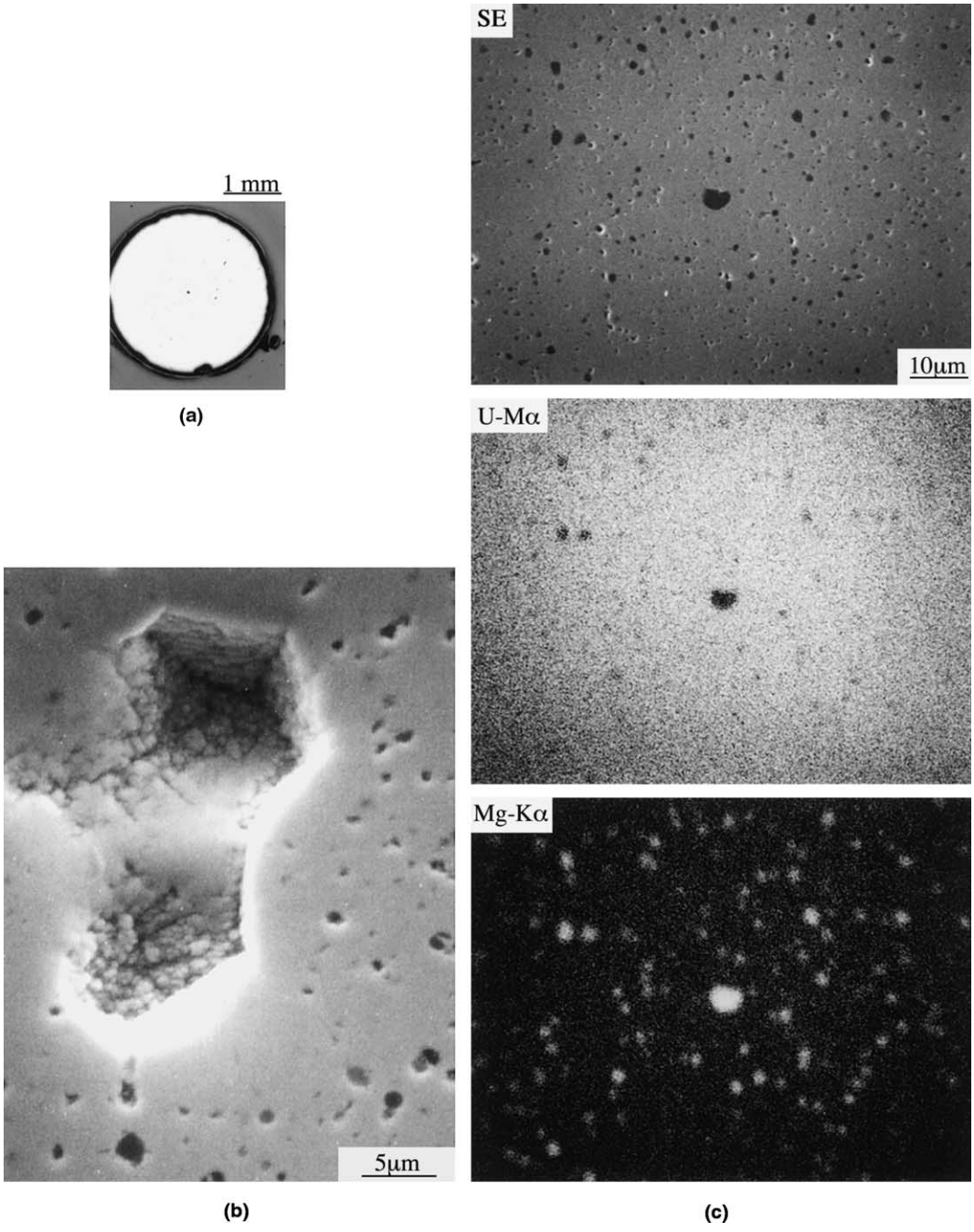

Fig. 13. Microstructure of 5%Mg–UO_2 pellet (F-4) irradiated to 53 GWd/tU at 560–600°C: (a) ceramograph; (b) SEM micrograph; (c) EPMA.

ture. The MgO particles seen before irradiation still existed. However, a part of the magnesium atoms were found to diffuse into the UO_2 matrix. Fig. 16(c) shows the SEM photographs of many small pores and a part of a large bubble formed. The lower left shows the surface of the large bubble where the typical rim structures were formed.

The effect of high temperature irradiation at 820–930°C was examined for I-10 and 11 samples (15%Mg–UO_2) of which the burnup was 63–64 GWd/

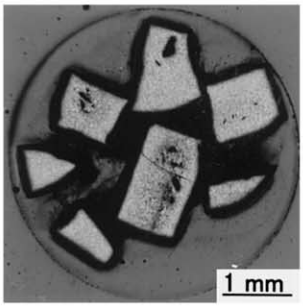

(a)

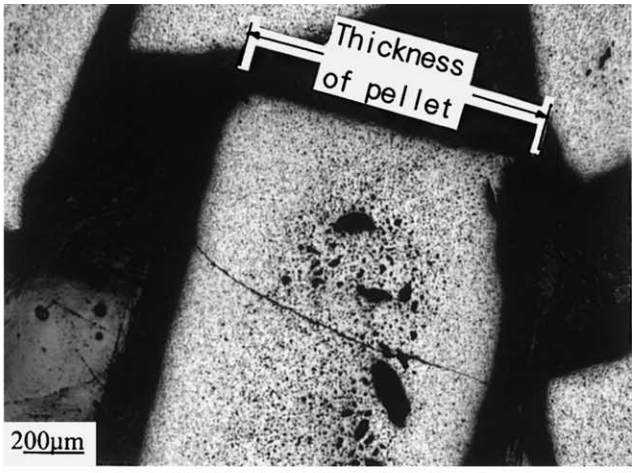

(b)

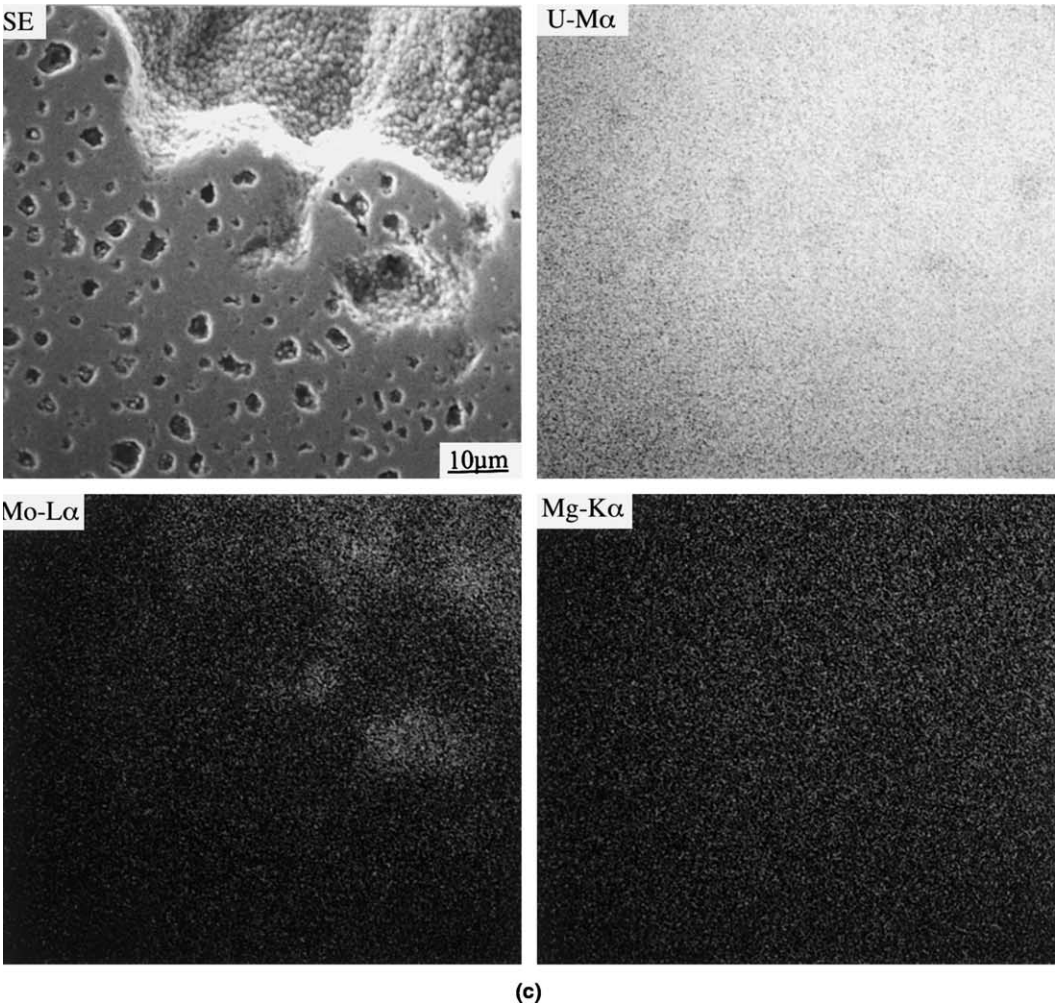

(c)

Fig. 14. High burnup irradiation of 5%Mg–UO_2: (a) fragments of E-13 pellet (91 GWd/tU, 600–650°C); (b) magnified ceramograph; (c) EPMA photographs.

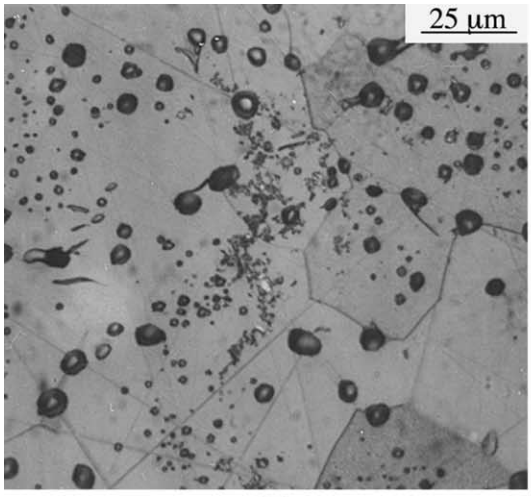

(a)

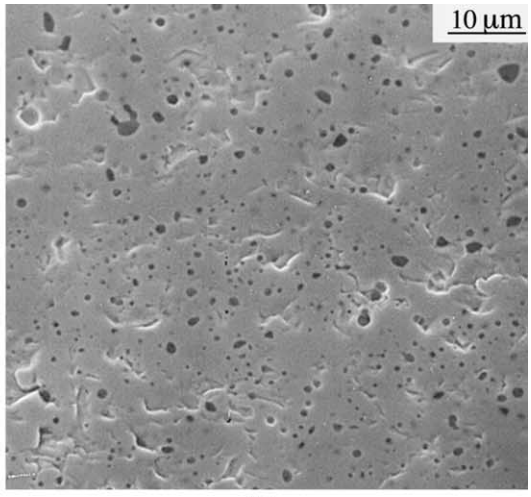

(b)

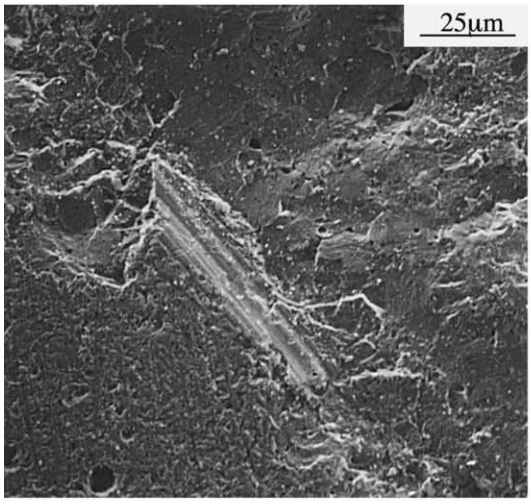

(c)

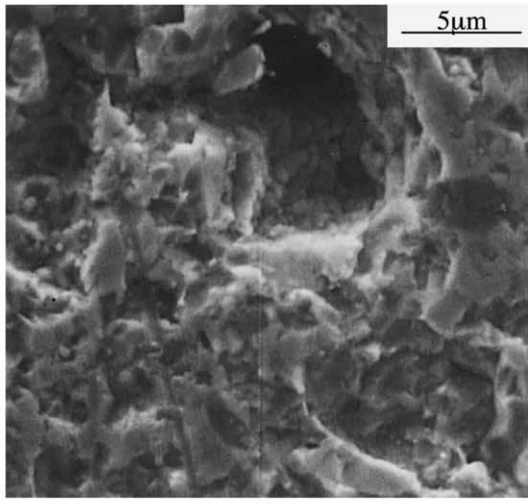

(d)

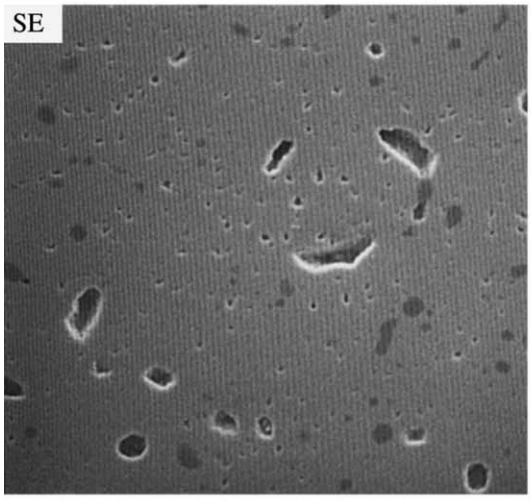

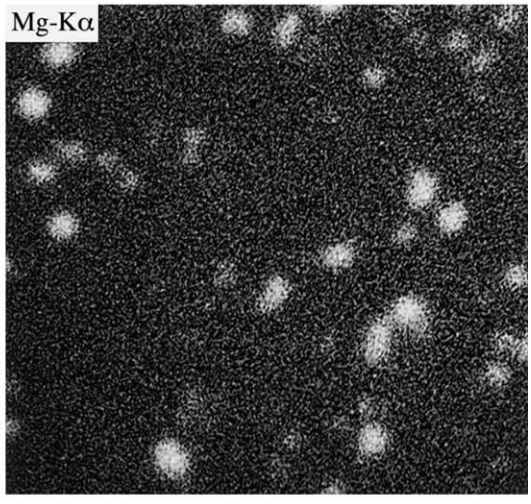

(e)

tU. The pellets were finely fractured. Observation of the large bubble of 120–180 μm diameter by SEM revealed that the dimension of the grains was not very changed by irradiation as shown in Fig. 17(a). Restructuring with sub-divided grains was not observed. Also, the porosity increase by large bubble formation did not occur. By the analysis of the elements in the matrix (Fig. 17(b)), it was shown that the MgO precipitates disappeared in the irradiated sample. Instead, an increased proportion of magnesium migrated into the grain boundaries (Mg–Kα). The metallic fission products were seen to precipitate as spot-like white inclusions. This behavior is represented by the EPMA photographs of Mo–Lα and Pd–Lα in Fig. 17(b).

5.5.3. 5%Mg–5%Nb–UO_2

In the unirradiated 5%Mg–5%Nb–UO_2 pellet, most of magnesium and niobium were precipitated at the grain boundaries of UO_2. The SEM micrograph of unirradiated 5%Mg–5%Nb–UO_2 is shown in Fig. 18(a). This structure is compared with that in the micrographs of the irradiated F-6 sample (55 GWd/tU, 560–600°C) shown in Figs. 18(b)–(d). The irradiated pellet was cracked into two large pieces during irradiation. A number of large pores observed in Fig. 18(b) are those formed on pellet preparation. The SEM micrograph of Fig. 18(c) shows the bubble inside by higher magnification, where the grains of 20–30 μm and their surface restructuring in the way to form the sub-divided grains can be observed. In the EPMA photographs of Fig. 18(d), magnesium and niobium were precipitated along the grain boundaries, same as in the unirradiated sample. However, the significant amount of these elements also migrated into the grains. Perhaps, the irradiation enhanced diffusion of them occurred in the sample. The metallic fission products (Mo, Tc, Ru, Rh and Pd) were confirmed to distribute uniformly in the UO_2 matrix.

5.5.4. 3.5%Ti–UO_2

The fragments of H-14, 15, 16, 17 samples irradiated to 66 GWd/tU burnup in the high temperature region (820–930°C) are shown in Fig. 19(a). The higher magnification ceramograph around the point A position of Fig. 19(a) is given in Fig. 19(b). The white inclusions of metallic fission products (Mo, Tc, Ru, Rh and Pd) are formed together with the bubbles grown up from the grain boundaries.

For the samples (B-15, 16, 17) of a higher burnup of 84 GWd/tU at lower temperature (570–640°C), the

(a)

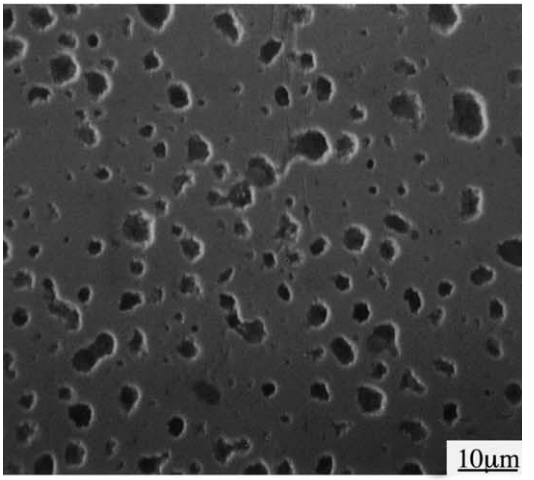

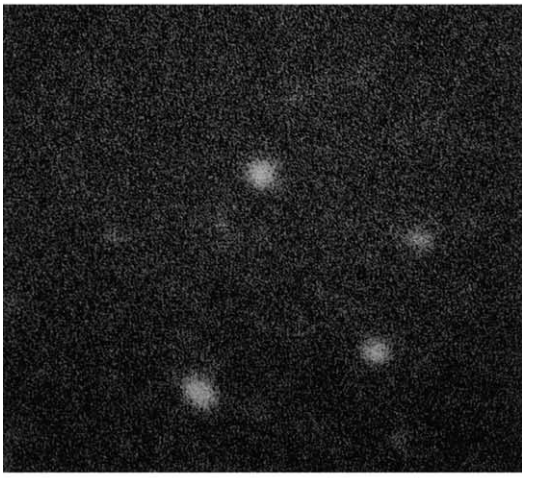

(b)

Fig. 16. High burnup 15%Mg–UO_2 pellet (F-13) (91 GWd/tU, 600–650°C): (a) ceramograph; (b) EPMA; (c) SEM micrographs of different magnifications.

Fig. 15. Microstructure of 15%Mg–UO_2: (a) ceramograph of unirradiated etched specimen; (b) SEM micrograph of unirradiated 15%Mg–UO_2; (c) ceramograph of sample A-6 (61 GWd/tU, 550–640°C); (d) SEM micrograph of sample A-6; (e) EPMA of sample A-6.

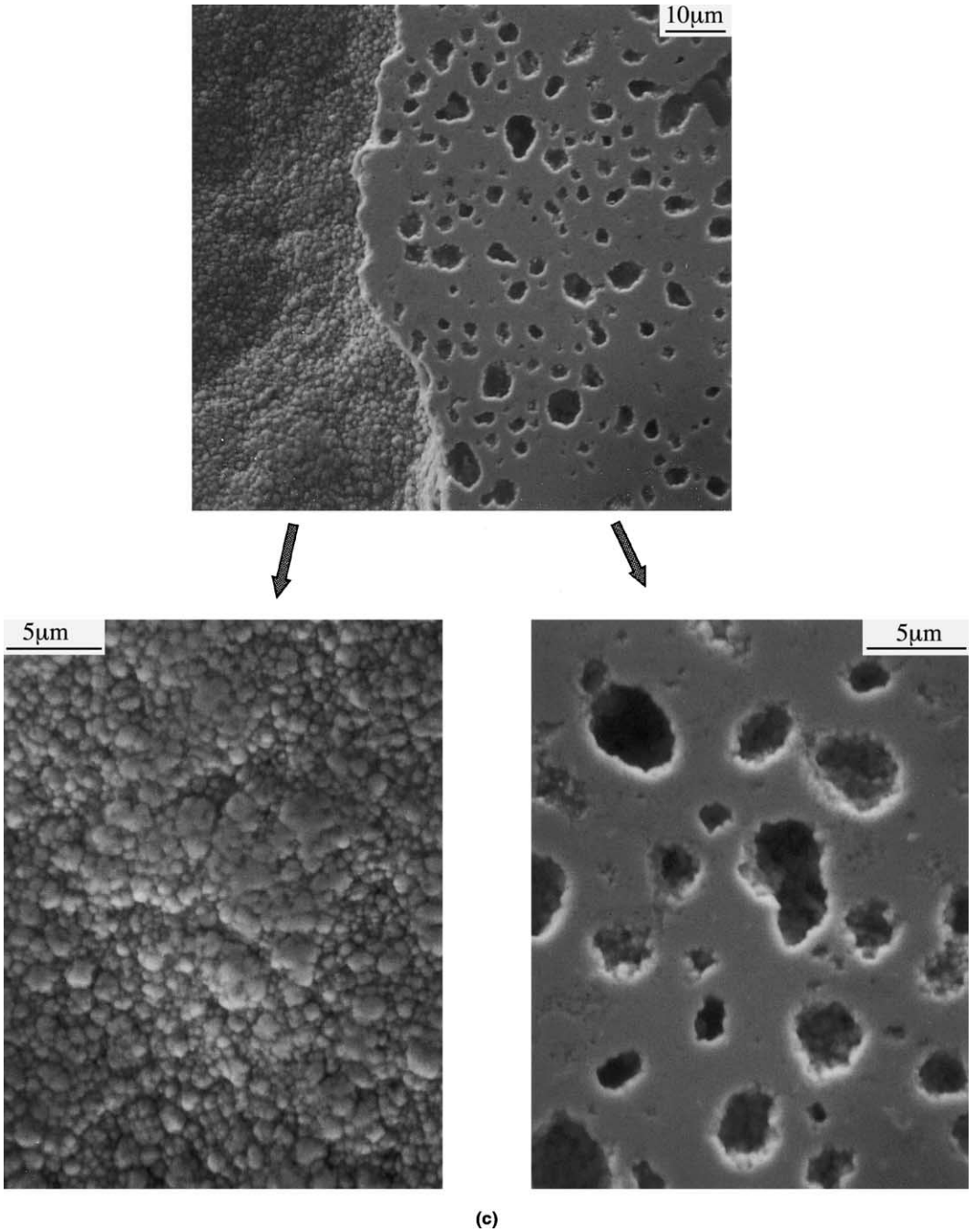

Fig. 16. (Continued).

fragments are shown in Fig. 20(a). The SEM micrograph of Fig. 20(b) indicates the large bubbles with rim structure. Fig. 20(c) shows the large bubble of 120–140 μm diameter. On this surface, a large number of subdivided grains of sub-micron size are seen. The qualitative determination of uranium and titanium by EPMA at the grain boundaries in the region of rim structure formation is shown in Fig. 20(d). Titanium was precipitated along the grain boundaries almost unchanged from that before irradiation, but in addition large bubbles were accumulated in the grain boundaries together with titanium. The metallic fission products were uni-

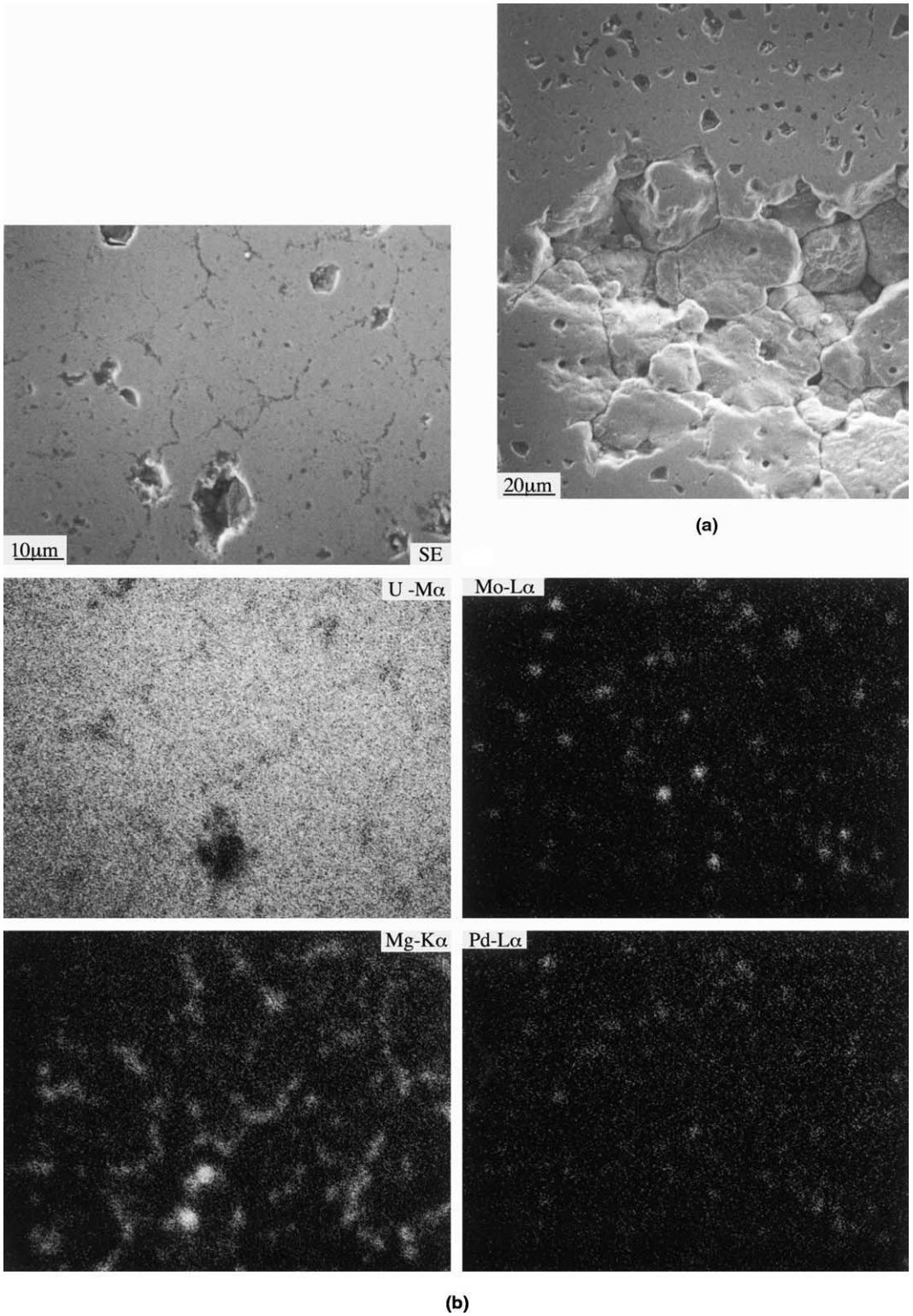

Fig. 17. High temperature irradiation of 15%Mg–UO_2 (I-10,11): (a) SEM micrograph (63–64 GWd/tU, 820–930°C); (b) EPMA.

formly distributed in the UO_2 matrix without forming precipitates.

6. Fission gas release

The migration and release of fission gas during irradiation were studied by measuring the retention of cerium, xenon and cesium in the UO_2 solid matrix. The amount of these fission products was represented by the intensity ratio (A/U) of the characteristic X-rays of the fission product element, A, to uranium. The measurements were carried out at every 250 μm directing from the surface to the radial center. The spot diameter used for the measurement was 5–6 μm. An example of the characteristic X-ray peaks of cerium, xenon, cesium and uranium in the EPMA pattern is given in Fig. 21 for specimen D-4.

The X-ray intensity ratios of Ce/U, Xe/U and Cs/U for the undoped UO_2 sample (Fig. 10) of 51 GWd/tU burnup in the lower temperature region (560–600°C) are plotted against the distance from the pellet radial surface in Fig. 22 by filled marks. The measured sample pellet was intact with its appearance very similar to the pellet before irradiation though the sub-divided grains were observed when closely examined.

The intensity ratio for Ce/U should be unvaried with the distance from surface if the burnup is uniform, since cerium does not migrate with temperature gradient even if it exists. That is to say, the positional change of burnup can be checked by the Ce/U ratio. The ratio in Fig. 22 is regarded as basically unchanged with distance from the pellet edge. The Ce/U ratios are in a band of 0.4–0.5, showing that the error is relatively large due to the small spot diameter adopted in the present measurements. The burnup can be regarded as uniform in the radial direction of the pellet, which is consistent with the present irradiation setup placing no moderator water outside the capsule, differed from the irradiation condition in LWR. The Xe/U and Cs/U X-ray intensity ratios were supposed to change with the distance if there was a significant temperature gradient. In Fig. 22, no significant correlation with distance was observed. It means that the radial temperature change was small if any in the pellet. The theoretical Xe/U intensity ratio of the characteristic X-rays was calculated to be 0.55 for the burnup of 51 GWd/tU. The observed Xe/U intensity ratios in Fig. 22 between 0.42 and 0.55, therefore, show the retention of xenon in the UO_2 matrix to be 0.76–1.0. The intensity ratio for cesium, Cs/U, was in the range from 0.42 to 0.51, giving no systematic change with distance.

The burnup of the F-4 specimen of 5%Mg–UO_2 (Fig. 13) was 53 GWd/tU (560–600°C). The sample pellet was intact without fracturing. Because the X-ray intensity ratios of Ce/U and Cs/U did not systematically change with distance, only the Xe/U intensity ratios are given in

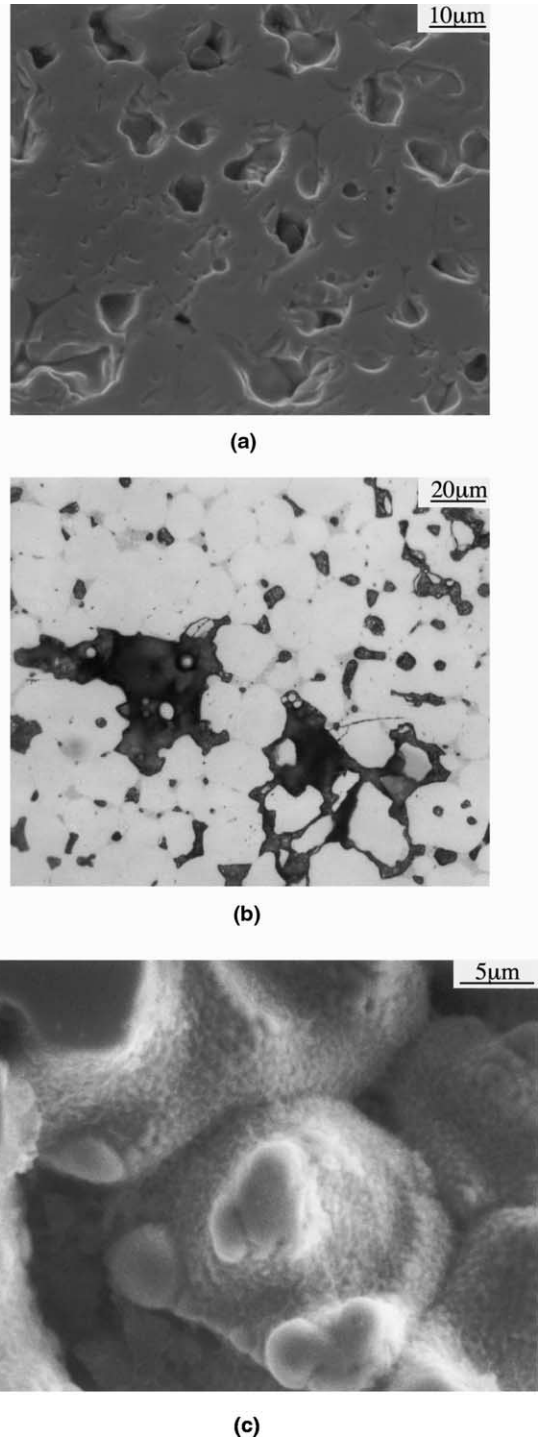

Fig. 18. Microstructure of 5%Mg–5%Nb–UO_2: (a) SEM micrograph of unirradiated 5%Mg–5%Nb–UO_2; (b) SEM micrograph of irradiated sample F-6 (55 GWd/tU, 560–600°C); (c) SEM micrograph of higher magnification; (d) EPMA.

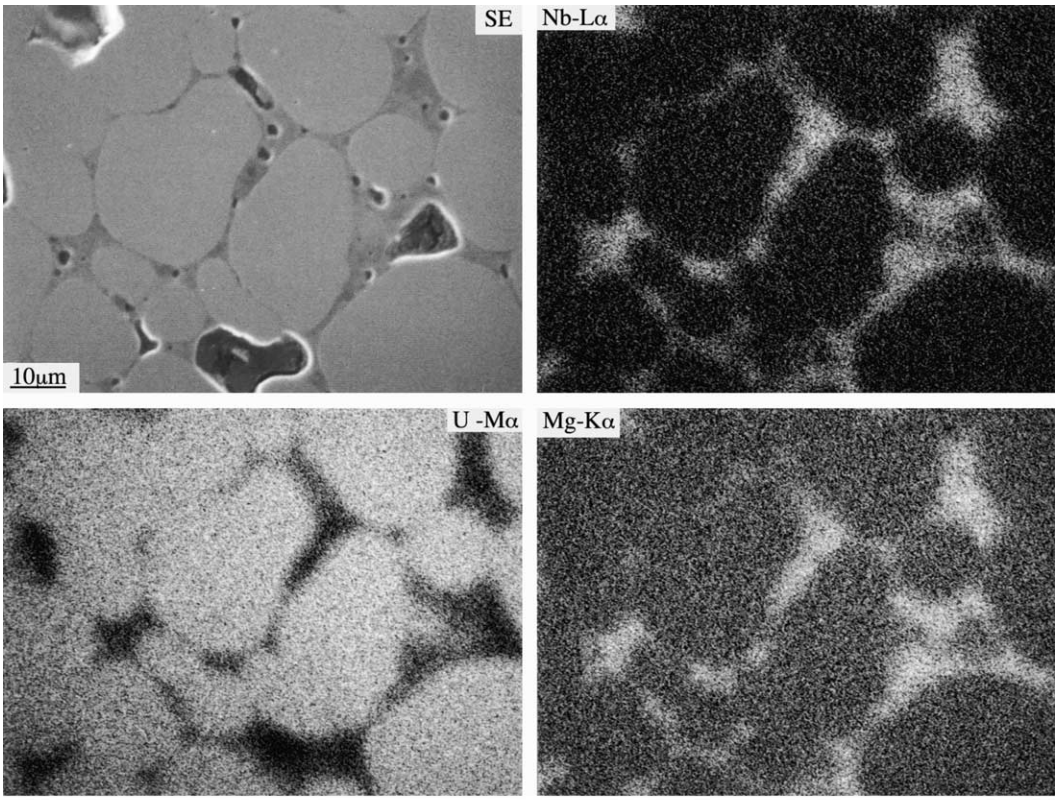

(d)

Fig. 18. (Continued).

Fig. 22. For 5%Mg–UO_2, these measured ratios were given by ◇ in the figure. No distance dependence of the Ce/U and Cs/U intensity ratios was also observed for the 5%Mg–5%Nb–UO_2 sample irradiated to 55 GWd/tU at the lower temperatures of 560–600°C (F-6, Fig. 18), for which thus only the Xe/U intensity ratios were plotted in Fig. 22.

It is seen from the figure that the Xe/U intensity ratio for 5%Mg–UO_2 largely fluctuates between 0.24 and 0.39. The measured ratios are smaller than those for undoped UO_2 (51 GWd/tU, 560–600°C). The calculated Xe/U ratio for 100% xenon retention in the matrix was 0.57 for 53 GWd/tU. The retention (fraction of xenon in the fuel matrix) is obtained by dividing the measured Xe/U ratio by the theoretical Xe/U ratio. Then, the xenon retention in the sample becomes 0.42–0.68. On the other hand, the Xe/U intensity ratio for the 5%Mg–5%Nb–UO_2 sample showed the smaller fluctuation in the range 0.49–0.54 which are the same or rather higher than the values for the above undoped UO_2. The xenon retention in the 5%Mg–5%Nb–UO_2 sample is estimated to be 0.83–1.0. As for the xenon retentions for the above three oxides of undoped UO_2, 5%Mg–UO_2 and 5%Mg–5%Nb–UO_2, however, it is difficult to discuss clearly their difference. The phenomenon is assumed to be related to the temperatures near 600°C, where the xenon retention changes rapidly as will be shown in Fig. 24.

The Xe/U X-ray intensity ratios measured for undoped UO_2 irradiated to 62 GWd/tU at high temperatures of 820–930°C were not shown in Fig. 22, since this pellet (G-9, Fig. 12) was fractured into many small pieces during irradiation and the distances from the surface could not be specified. However, the acquisition of two data was made for this fuel. Their Xe/U intensity ratios were much smaller, i.e. 0.099 and 0.119. The calculated ratio for 100% retention estimated for 62 GWd/tU was 0.65. Therefore, the xenon retentions in the matrix are obtained as 0.15 and 0.18. Such very low values for the above specimens irradiated at high temperature demonstrate that the temperature is a very important factor of the xenon gas release.

In Fig. 23, the intensity ratios are plotted against the distance from the disk periphery for high burnup samples. The undoped UO_2 pellets of D-9, 10 and E-9, 10 were those irradiated to 87–94 GWd/tU at 560–600°C.

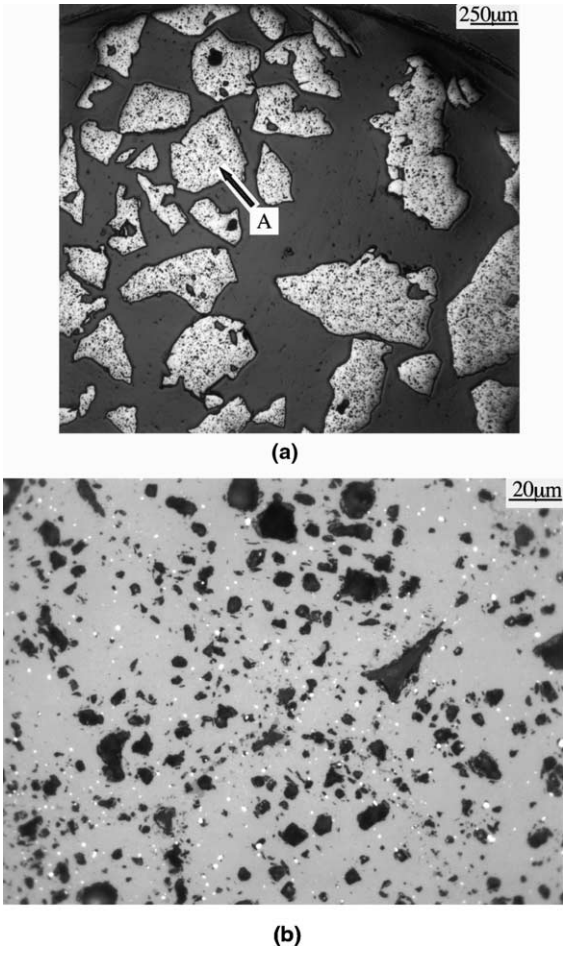

Fig. 19. High temperature irradiation of 3.5%Ti–UO_2 (H-14,15,16, 17): (a) fragments of samples H-14,15,16,17 after irradiated to 66 GWd/tU at 820–930°C; (b) higher magnified ceramograph of the arrow point of (a).

They were broken into large pieces (Fig. 11), from which two samples I and II were taken out for X-ray intensity measurement. Sample I exhibited coalesce of larger bubbles in the inner region compared with usual large pores formed near the outer rim region. In sample II, on the other hand, the rim structure was widely spread with relatively small pores of <5 μm which were distributed uniformly from the outer surface to the central part of the pellet. The measured Xe/U intensity ratio shown in Fig. 23 for sample I is higher in the outer region (short distances), while it falls down to ~0.2 in the inner region where the larger pores coalesced. The Xe/U intensity ratio for sample II also seemed to change with distance though intensity behavior was not the same. Namely, the X-ray intensity ratio increased toward the central part. The minimum and the maximum intensity ratios throughout samples I and II were obtained as 0.17 and 0.44, respectively. The calculated Xe/U ratio at 90 GWd/tU for 100% retention is 0.90. Thus, the above two values give the xenon retentions of 0.19 and 0.49 in the UO_2 matrix. The ratios of X-ray intensities of Ce/U and Cs/U are plotted in Fig. 23 for sample II but not for sample I because there was no significant difference in these values for the two samples. As seen from the figure, both the Ce/U and Cs/U ratios do not change systematically with distance, in accordance with those for the irradiated samples of the 51–62 GWd/tU range as already described. The ratios of Ce/U were in the range 0.66–0.73, and those of Cs/U 0.62–0.74. These ratios are higher due to the high burnup of the samples. Because it was shown by the above Ce/U and Cs/U ratios that the burnup and temperature of the pellets are essentially independent of the distance from the periphery, the difference in the Xe/U ratios for samples I and II is considered to be ascribed to the fluctuation of the measured values. Une et al. [55] have irradiated the undoped UO_2 disks to high burnups in JRR-3M. According to their result, the xenon retention was flat with respect to distance for the specimens of 90 GWd/tU burnup at about 550°C. The retention of this work is in good ageement with their value, 0.32.

The 5%Mg–UO_2 pellet (E-13, Fig. 14) of 91 GWd/tU burnup (600–650°C) was fragmented into several pieces. As mentioned above, the rim structure was developed and the large bubbles have emerged in the region apart from the pellet edge. Fig. 23 shows that the intensity ratios of Ce/U and Cs/U and their distance dependence were close to those of irradiated undoped UO_2 (samples I and II). The Xe/U intensity ratios were in a range 0.18–0.28. Taking into account the error in the measurements, it can be regarded that the Xe/U ratios for 5%Mg–UO_2 are the same as those of undoped UO_2.

The 15%Mg–UO_2 pellet irradiated to 91 GWd/tU at 600–650°C (F-13, Fig. 16) was cracked into two pieces. As described in Section 5.5.2, the surface of this pellet was all covered with the rim structure. As in the case of the other samples, the intensity ratios for Ce/U and Cs/U did not change significantly with the distance from the outer surface (Fig. 23). The Ce/U ratio was 0.67 at the pellet edge and it was 0.59 at the central part. The Xe/U intensity ratios for this sample were in a range 0.11–0.19. These ratios would yield the xenon retentions of 0.13–0.21 (average 0.17) which are somewhat lower than those of the undoped UO_2 (87–94 GWd/tU, 560–600°C). However, the meaning of this difference is vague because of large scattering of the measured points. An interesting result seen at the position 1000 μm distant from the surface of the 15%Mg–UO_2 pellet is that the sub-divided grains were formed on a very large bubble at this point, whereas no definite changes were detected in the intensity ratios as shown in Fig. 23. It is possible that below such subgrains there extends a region of structures which gives the intensity ratios virtually the same as those of normal grains.

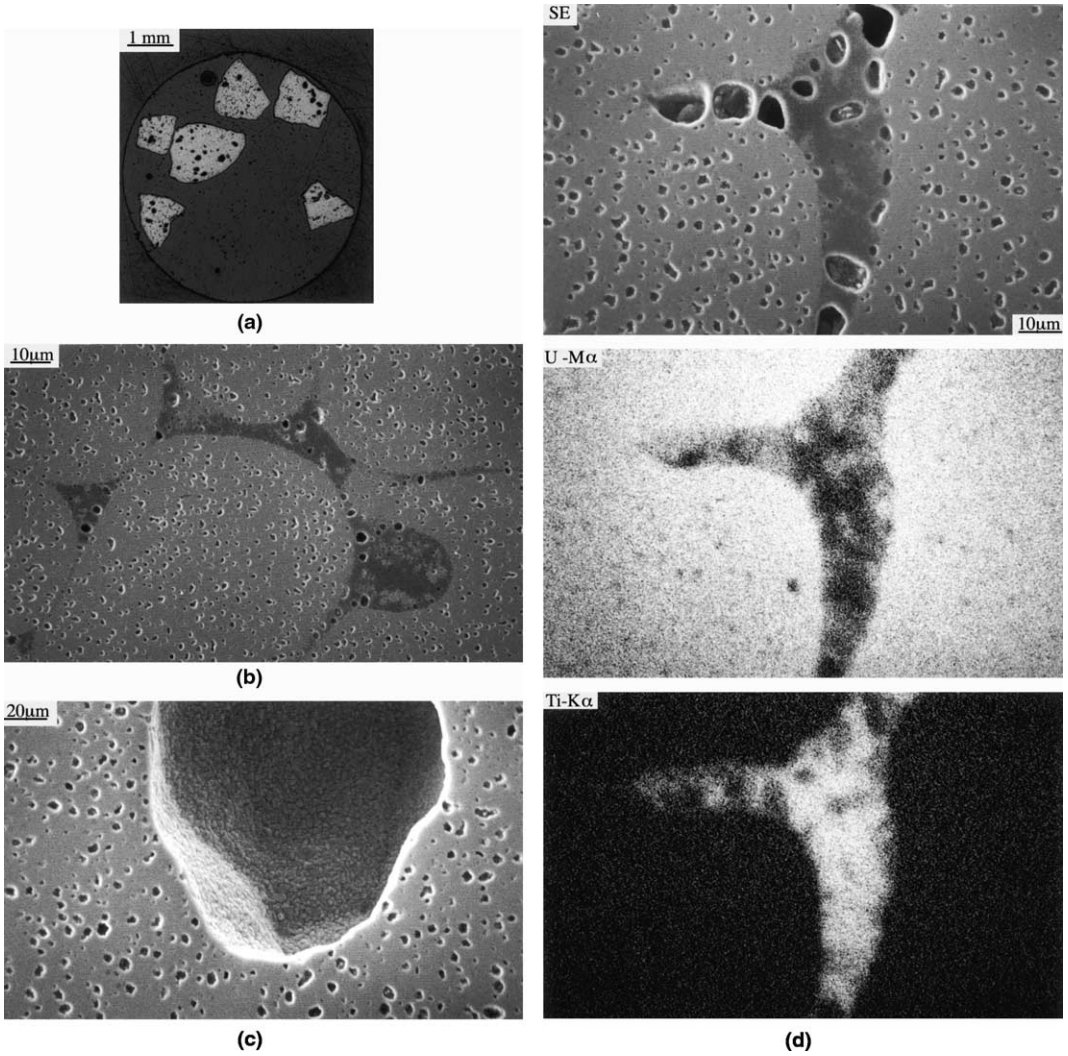

Fig. 20. High burnup 3.5%Ti–UO_2 at lower temperature (570–640°C): (a) fragments of samples B-15,16,17 with burnup 84 GWd/tU; (b) SEM micrograph; (c) SEM micrograph of the large bubble with 120–140 μm diameter; (d) EPMA photographs showing titanium precipitation along the grain boundaries.

The 3.5%Ti–UO_2 pellet was fragmented into many small pieces after irradiated to 84 GWd/tU at 570–640°C. Measurements of the ratios were made for one point of a piece of this sample. The measured ratios were not shown in Fig. 23 because the distance could not be specified. The measured Ce/U and Cs/U intensity ratios obtained were 0.74 and 0.67, respectively. These ratios are consistent with those of the other samples in this work. The Xe/U intensity ratio was measured as 0.29, which can be regarded as in line with those of the other samples shown in Fig. 23.

In the burnup range 51–62 GWd/tU, the large difference in the characteristic X-ray intensity ratios, Xe/U, for the two undoped UO_2 samples was noticed. In Fig. 24, the retention of xenon in the oxide matrix during irradiation is represented as a function of temperature. Since the temperature of the sample was changed within a certain width during irradiation, the middle point in the width was adopted as the temperature in the figure. The undoped UO_2 sample irradiated to 51 GWd/tU at temperatures between 560°C and 600°C gave the high xenon retention of 0.76–1.0 (average 0.88). On the other hand, the undoped UO_2 sample irradiated to 62 GWd/tU at higher temperatures of 820–930°C gave the xenon retentions as low as 0.15–0.18 (average 0.17). These values are shown by open circles. The discrepancy in the above ratios is considered to be caused primarily by the temperature on irradiation. The filled circles in Fig. 24

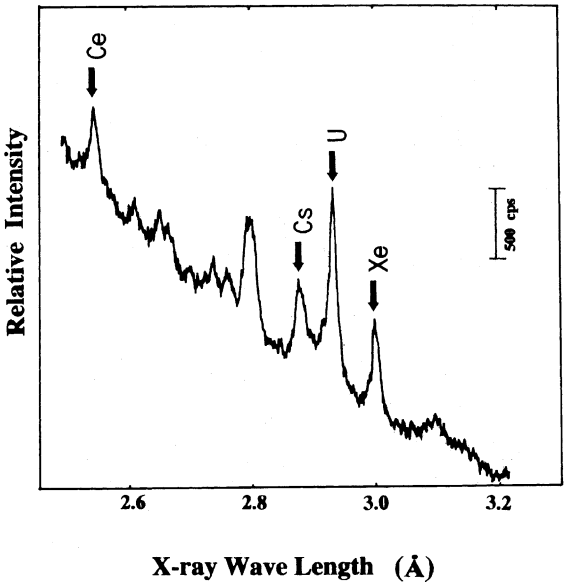

Fig. 21. Typical characteristic X-ray pattern of fission products in irradiated sample measured by EPMA (Sample: D-4).

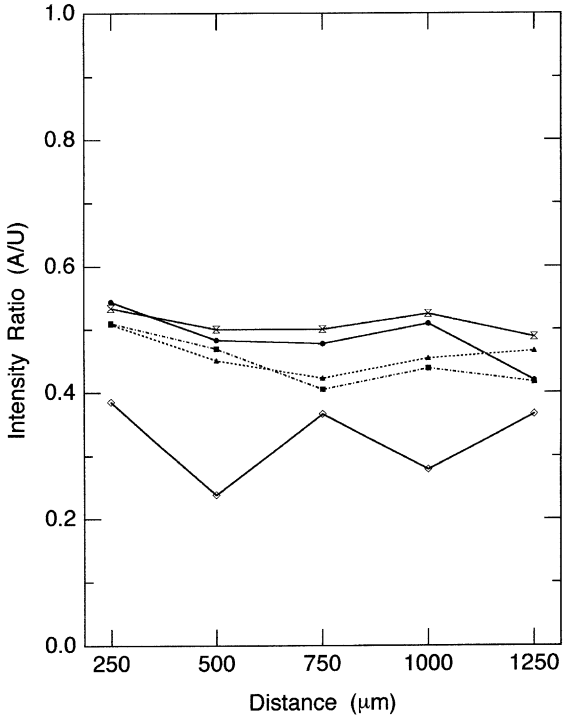

Fig. 22. Intensity ratios (A/U; A = Xe, Ce, Cs) of characteristic X-rays of the elements against the distance from the outer surface for the irradiated samples in a range of burnups 51–62 GWd/tU: (—●—) Xe/U for undoped UO_2 (51 GWd/tU, 560–600°C); (···■···) Ce/U for undoped UO_2; (···▲···) Cs/U for undoped UO_2; (—◇—) Xe/U for 5%Mg–UO_2 (53 GWd/tU, 600–650°C); (—⧖—) Xe/U for 5%Mg–5%Nb–UO_2 (55 GWd/tU, 560–600°C).

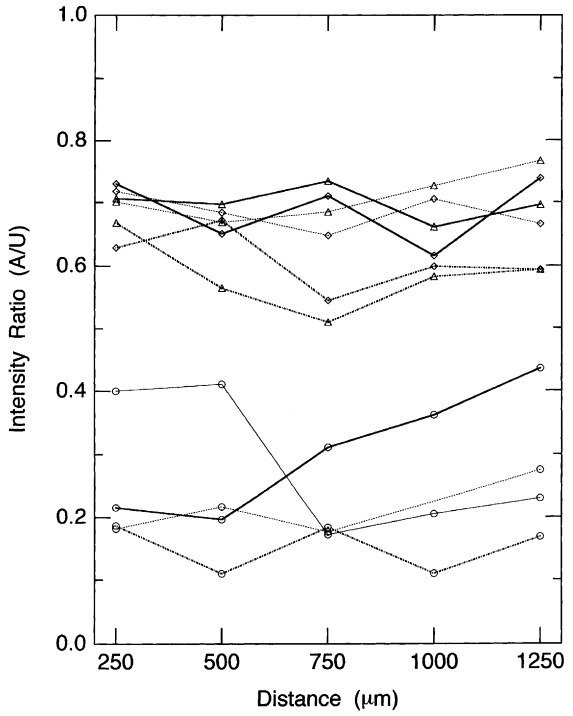

Fig. 23. Intensity ratios (A/U; A = Xe, Ce, Cs) of characteristic X-rays of the elements against the distance from the outer surface for the irradiated samples in a range of burnups 87–94 GWd/tU: (—○—) Xe/U for undoped UO_2, Sample I (87–94 GWd/tU, 560–600°C); (—○—) Xe/U for undoped UO_2, Sample II (87–94 GWd/tU, 560–600°C); (···○···) Xe/U for 5%Mg–UO_2 (91 GWd/tU, 600–650°C); (-·○-·) Xe/U for 15%Mg–UO_2 (91 GWd/tU, 600–650°C); (—△—) Ce/U for undoped UO_2, Sample II; (···△···) Ce/U for 5%Mg–UO_2; (-·△-·) Ce/U for 15%Mg–UO_2; (—◇—) Cs/U for undoped UO_2, Sample II; (···◇···) Cs/U for 5%Mg–UO_2; (-·◇-·) Cs/U for 15%Mg–UO_2.

show the retention for 5%Mg–UO_2 (53 GWd/tU, 560–600°C) and 5%Mg–5%Nb–UO_2 (55 GWd/tU, 560–600°C) samples. The solid curve indicates the variation of the retention of xenon with temperature, where the difference of burnup in the 51–62 GWd/tU range was disregarded. Except for undoped UO_2 (62 GWd/tU) irradiated at high temperatures of 820–930°C, the burnup only slightly differed within 51 and 55 GWd/tU in the other irradiated samples of undoped UO_2, 5%Mg–UO_2 and 5%Mg–5%Nb–UO_2. The lower open circle for 62 GWd/tU undoped UO_2 could move upward to some extent on correction of burnup.

Fig. 24 shows that the xenon retention sharply decreases with increasing temperature above 600°C, and then the change becomes smaller above 700°C. The latter levelling off may be because most xenon has already been released from the solid at higher temperatures. The broken line in the figure shows the change of

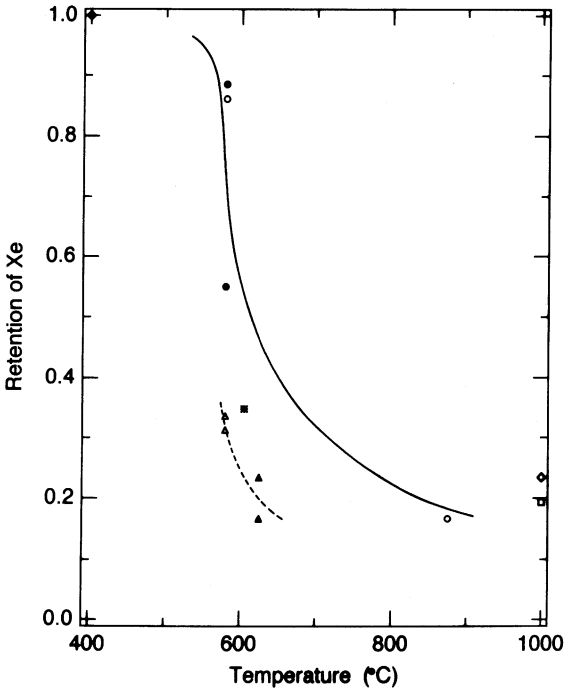

Fig. 24. Variation of xenon retention in the UO_2 matrix with temperature: (○) undoped UO_2 in the 51–62 GWd/tU burnup range (upper, 51 GWd/tU, 560–600°C; lower, 62 GWd/tU, 820–930°C); (●) 5%Mg–5%Nb–UO_2 and 5%Mg–UO_2 in the 51–62 GWd/tU burnup range (upper, 5%Mg–5%Nb–UO_2, 55 GWd/tU, 560–600°C); lower, 5%Mg–UO_2, 560–600°C; (◇) undoped UO_2 literature value at 50 GWd/tU [39]; (△) undoped UO_2 in the 87–94 GWd/tU burnup range (560–600°C); (▲) 5%Mg–UO_2 and 15%Mg–UO_2 in the 87–94 GWd/tU burnup range (upper, 5%Mg–UO_2, 91 GWd/tU, 600–650°C; lower, 15%Mg–UO_2, 91 GWd/tU, 600–650°C); (✳) 3.5%Ti–UO_2 at 84 GWd/tU (570–640°C); (□) undoped UO_2 literature value at 83 GWd/tU [39].

the xenon retention with temperature for the high burnup samples of 87–94 GWd/tU. For this plot also, the middle point temperatures of the fluctuation during irradiation were taken as the sample temperatures. Clearly, the xenon retention in the figure greatly lowered with increasing burnup. The open triangles in the figure depict the xenon retention for the undoped UO_2 samples of I and II (87–94 GWd/tU, 560–600°C). The filled triangles give the retention for the 5%Mg–UO_2 (91 GWd/tU, 600–650°C) and 15%Mg–UO_2 (91 GWd/tU, 600–650°C) samples. The retention of 3.5%Ti–UO_2 (84 GWd/tU, 570–640°C) is higher than the broken line. This upward shift can be explained by a lower burnup of this sample.

If the tentative two curves above really express the variation of retention of xenon (or xenon gas release), the main factors affecting the retention are to be the irradiation temperature and burnup. The slope of the solid curve in Fig. 24 becomes much gentler below 600°C. It is possible that the solid curve converges more rapidly to 1 as the temperature decreases from 600°C.

The ◇ marks in Fig. 24 are the EPMA values reported by Manzel and Walker [39] for the PWR fuel pellets irradiated to 50 GWd/tU. The mark at left upmost indicates the xenon retention at pellet periphery. Because the periphery temperature was not given in the paper, 400°C was assigned tentatively. This retention seems to be well connected with the solid line. At the central part of the above pellet, the xenon retention was 0.23 [39]. In Fig. 24, this literature value is given against the tentatively supposed temperature, 1000°C, because no information was given about the temperature. For this xenon retention, the solid line gives about 800°C. According to the analysis of inpile BWR fuel temperature [56], the fuel center temperature was around 800°C if the local heat rate was 180 W/cm. It should be taken into account that the fuel temperature in their experiment was high at the earlier stage of irradiation with the linear heat rate of 260–290 W/cm at 29–37 GWd/tU.

For the disks irradiated under nearly the same conditions as the present work, Une et al. [55] have found that the porosity was higher and the bubble size was larger than those of LWR fuel though the xenon depression and the rim structure formation were alike. These experimental results were thought to be related with the restraint pressure [55]. The unvaried xenon depression in their report may have been obtained as a result of the lower temperature (550°C). The release of xenon is considered to occur significantly from the unconstrained fuel above 800°C. As for the present xenon retention of 0.17 for the 62 GWd/tU irradiated undoped UO_2 sample (820–930°C), there remains a possibility that the temperature was actually near 1000°C, though the error in the specimens has been estimated to be generally ±50°C.

The literature value for the xenon retention at the central part of the 83 GWd/tU irradiated fuel pellet is 0.194 [39], which is given as the □ mark in Fig. 24 at the supposed temperature of 1000°C. The broken line for high burnup fuels in the figure does not give a good connection with this release fraction. This misfit may be ascribed to the lower xenon retention in the unconstrained present fuel.

Although the formation of rim structure has been reported for the BWR fuel of 48 GWd/tU [57] or for the PWR fuel of 49 GWd/tU [58], the rim structure was not detected for all the fuel pellets in the 51–62 GWd/tU burnup range in this work concerned to the solid line in Fig. 24. In the work for the pellets with no radial temperature and burnup gradients, it has been reported that the rim structure was not formed at the burnup of 55 GWd/tU (410–430°C). The threshold burnup of the rim structure formation has been evaluated to be usually between 55 and 82 GWd/tU [59] in accordance with the

present results. However, in our samples of the 51–62 GWd/tU burnup range, the symptom of commencement of restructuring (grain sub-division) was detected. This result is also consistent with the reports [59,60].

The effect of addition of metal oxides on fission gas release seems to become small or subsidiary at high burnups. The large addition effects were not observed here for 5%Mg–UO_2, 15%Mg–UO_2, 5%Mg–5%Nb–UO_2 and 3.5%Ti–UO_2 specimens. However, it should be mentioned that the sample dimension and the irradiation condition in this work were very different from those of the oxide fuels in LWRs. The present experiments are supposed to give especially useful information on irradiation phenomena near the pellet periphery of the LWR fuel at high burnups. That is to say, the irradiation temperature was not changed over the whole pellet surface in the present samples, and the wide surface of each pellet was in contact with the gas phase. For discussing closely the effect of metal addition, acquisition of more data of post-irradiation examinations for the high burnup fuels irradiated under the LWR condition is desired.

A large number of studies have been made or are now being carried out with the aim to reduce the release of fission gas by adding metal oxides. They are, for example, TiO_2 [7–11], Nb_2O_5 [9,12–14], V_2O_5 [9,15], Cr_2O_3 [16,17], La_2O_3 [12], MgO [7,17], CaO–TiO_2 [18,19]. Sawbridge et al. [21] reported that the fission gas release was reduced by a factor of 2.5 for the 5 mol% MgO doped fuel when it was irradiated to 28.5 GWd/tU. According to the result for high burnup fuels in this work, the matrix of the pellet oxides was heavily damaged, and both compositional and structural changes took place. The present fission gas release behavior could be analyzed as the phenomenon associated with the above damaged structures which is considered to be annealed faster at high temperatures.

Here the addition of magnesium was shown to be hopeful for having a high burnup solid solution fuel. When magnesium is doped in UO_2, change occurs in the important physico-chemical properties for the fuel performance, viz. oxygen potential, thermal conductivity, plasticity and so on. For closer elucidation of the irradiation effect of the doped fuels, acquisition of more property data in relation with the post-irradiation experiments is awaited.

Acknowledgements

The authors express their thanks to Dr Kimio Hayashi and Mr. Masao Aizawa and staff of Hot Laboratory of Japan Atomic Energy Research Institute for post-irradiation examinations and helpful discussions on the results.

References

[1] T.B. Lindemer, A.L. Sutton Jr., J. Am. Ceram. Soc. 71 (1988) 553.
[2] K. Une, M. Oguma, J. Nucl. Mater. 115 (1983) 84.
[3] A.E. Martin, R.K. Edwards, J. Phys. Chem. 69 (1965) 1788.
[4] R.E. Woodley, J. Nucl. Mater. 96 (1981) 5.
[5] J. Edwards, R.N. Wood, G.R. Chilton, J. Nucl. Mater. 130 (1985) 505.
[6] K. Une, M. Oguma, J. Nucl. Mater. 131 (1985) 88.
[7] K. Maruya, S. Takahashi, K. Yamamoto, Y. Honda, J. At. Energy Soc. Jpn. 5 (1963) 395.
[8] I. Amato, R.L. Columbo, A.P. Balzari, J. Nucl. Mater. 18 (1966) 252.
[9] G. Arthur, D. Scott, Trans. Br. Ceram. Soc. 63 (1964) 417.
[10] J.B. Ainscough, F. Rigby, S.C. Osborn, J. Nucl. Mater. 52 (1974) 191.
[11] K. Une, I. Tanabe, M. Oguma, J. Nucl. Mater. 150 (1987) 93.
[12] J.C. Killeen, J. Nucl. Mater. 58 (1975) 39.
[13] H. Assmann, W. Doerr, G. Gradel, G. Maier, M. Peehs, J. Nucl. Mater. 98 (1981) 216.
[14] K.W. Song, S.H. Kim, S.H. Na, Y.W. Lee, M.S. Yang, J. Nucl. Mater. 209 (1994) 280.
[15] I. Amato, M. Ravizza, R.L. Columbo, J. Nucl. Mater. 23 (1967) 103.
[16] J.C. Killeen, J. Nucl. Mater. 88 (1980) 177.
[17] S. Kashibe, K. Une, H. Masuda, Proc. 1996 Spring Meeting of Atomic Energy Soc. Jpn., Osaka, March 27–29, 1996, K35, p. 521.
[18] B.E. Schaner, Bull. Am. Ceram. Soc. 38 (1959) 494.
[19] K.C. Radford, J.M. Pope, J. Nucl. Mater. 116 (1983) 305.
[20] B.E. Ingleby, K. Hand, in: I.J. Hastlings (Ed.), Advances in Ceramics, vol. 17, Fission-Product Behavior in Ceramic Oxide Fuel, The American Ceramic Soc., Columbus, OH, 1986, p. 57.
[21] P.T. Sawbridge, C. Baker, R.M. Cornell, K.W. Jones, D. Reed, J.B. Ainscough, J. Nucl. Mater. 95 (1980) 119.
[22] T. Fujino, K. Naito, J. Inorg. Nucl. Chem. 32 (1970) 627.
[23] S. Kemmler-Sack, W. Rüdorff, Z. Anorg. Allg. Chem. 354 (1967) 255.
[24] J.S. Anderson, K.D.B. Johnson, J. Chem. Soc. 1731 (1953).
[25] Hj. Matzke, Private communication.
[26] T. Fujino, S. Nakama, N. Sato, K. Yamada, K. Fukuda, H. Serizawa, T. Shiratori, J. Nucl. Mater. 246 (1997) 150.
[27] T. Fujino, N. Sato, J. Nucl. Mater. 189 (1992) 103.
[28] T. Fujino, N. Sato, K. Yamada, J. Nucl. Mater. 223 (1995) 6.
[29] T. Fujino, N. Sato, K. Fukuda, Proc. 1997 Int. Topical Mtg. on LWR Fuel Performance, Portland, March 2–6, 1997, p. 565.
[30] T. Fujino, N. Sato, K. Yamada, T. Shiratori, K. Fukuda, H. Serizawa, in: Proc. 2000 Int. Tpoical Mtg. on LWR Fuel Performance, Park City, April 10–13, 2000, p. 641.
[31] F. Abbattista, P. Rolando, G.B. Grassi, Ann. Chim. (Rome) 60 (1970) 426.
[32] J.D.B. Lambert, R. Strain, Oxide fuels, in: B.R.T. Frost (Ed.), Materials Science and Technology, vol. 10A, Nuclear Materials, VCH, Weinheim, 1994, p. 137.
[33] K. Maruya, S. Takahashi, T. Watanabe, S. Ogura, J. At. Energy Soc. Jpn. 4 (1962) 845.
[34] B.J. Skinner, Am. Mineral. 42 (1957) 39.

[35] T. Fujino, N. Sato, K. Yamada, J. Nucl. Mater. 247 (1997) 265.
[36] H.C. Roland, AEC-Report, ORNL-TM-1942, 1967.
[37] M.L. Bleiberg, R.M. Berman, B. Lustman, AEC-Report, WAPD-T-1455, 1962.
[38] H. Assmann, R. Manzel, J. Nucl. Mater. 68 (1977) 360.
[39] R. Manzel, C.T. Walker, in: Proc. 2000 Int. Tpoical Mtg. on LWR Fuel Performance, Park City, April 10–13, 2000, p.752.
[40] J.B. Conway, R.M. Fincel Jr., R.A. Hein, Trans. ANS 6 (1963) 153.
[41] Y.S. Touloukian, K. Kirby, R.E. Taylor, T.Y.R. Lee, Thermophys. Properties of Matter, vol. 13, Thermal Expansion of Nonmetallic Solids, IFI/Plenum, New York, 1977, p. 288.
[42] I. Barin, O. Knacke, Thermochemical Properties of Inorganic Substances, vol. 813, Springer, Berlin, 1973, p. 441.
[43] C.S. Olsen, G.A. Reymann, in: P.E. MacDonald, L.B. Thompson (Eds.), A Handbook of Materials Properties for Use in the Analysis of Light Water Reactor Fuel Rod Behavior, AEC Report, TREE-NUREG-1005, 1976, p. 26.
[44] W.D. Kingery, in: Introduction to Ceramics, Wiley, New York, 1960, p. 507.
[45] J. Nakamura, T. Kodaira, M. Uchida, T. Yamahara, H. Uetsuka, A. Kikuchi, in: Proc. Int. Topical Mtg. on LWR Fuel Performance, Portland, March 2–6, 1997, p. 499.
[46] S.K. Yagnik, in: Proc. 2000 Int. Tpoical Mtg. on LWR Fuel Performance, Park City, April 10–13, 2000, p. 763.
[47] R.C. Daniel, I. Cohen, AEC Report, WAPD-246, 1964.
[48] M. Amaya, M. Hirai, J. Nucl. Mater. 247 (1997) 76.
[49] P.G. Klemens, Proc. Roy. Soc. London A 208 (1951) 108.
[50] Y. Takahashi, M. Murabayashi, J. Nucl. Sci. Technol. 12 (1975) 133.
[51] N. Nogita, K. Une, M. Hirai, K. Ito, Y. Shirai, J. Nucl. Mater. 248 (1997) 196.
[52] N. Lozano, L. Desgranges, D. Aymes, J.C. Niepce, J. Nucl. Mater. 257 (1998) 78.
[53] M. Kinoshita, T. Kameyama, S. Kitajima, Hj. Matzke, J. Nucl. Mater. 252 (1998) 71.
[54] M. Morgensen, J.H. Pearce, C.T. Walker, J. Nucl. Mater. 264 (1999) 99.
[55] K. Une, K. Nogita, Y. Suzawa, K. Hayashi, K. Ito, Y. Etoh, in: Proc. 2000 Int. Tpoical Mtg. on LWR Fuel Performance, Park City, April 10–13, 2000, p. 775.
[56] W. Wiesenack, T. Tverberg, in: Proc. 2000 Int. Tpoical Mtg. on LWR Fuel Performance, Park City, April 10–13, 2000, p. 730.
[57] K. Nogita, K. Une, J. Nucl. Mater. 226 (1995) 302.
[58] L.E. Thomas, C.E. Beyer, L.A. Chalot, J. Nucl. Mater. 188 (1992) 80.
[59] M. Kinoshita, T. Sonoda, S. Kitajima, A. Sasahara, E. Kolstad, Hj. Matzke, V.V. Rondinella, A.D. Stalios, C.T. Walker, I.L.F. Ray, M. Sheindlin, D. Halton, C. Ronchi, in: Proc. 2000 Int. Tpoical Mtg. on LWR Fuel Performance, Park City, April 10–13, 2000, p. 738.
[60] J. Spino, K. Vennix, M. Coquerell, J. Nucl. Mater. 231 (1996) 179.